Chapter 3

Chromium(III) Bidentate Nitrogen Ligand Chemistry

3.1 INTRODUCTION

Since its discovery at the end of the nineteenth century, the bipyridine ligand (commonly referred to as (bipy) has been used extensively in the complexation of metal ions. This particular aromatic nitrogen-containing heterocyclic ligand exhibits six possible region–isomeric forms – three symmetrical (2,2' , 3,3' , 4,4') and three asymmetrical (2,3' , 2,4' , 3,4'). The most common of these is the 2, 2' isomer. Due to its robust stability and ease of functionalisation, 2, 2'–bipyridine allows the formation of stable, rigid, five–membered chelate rings with the metal centre. Coordination takes place via the σ–donating nitrogen atoms [102].

As only two of the three available coordination sites are taken up, via substitution of the thf ligands in the $[CrCl_3(thf)_3]$ precursor, the addition of bipyridine allows the further addition of a monodentate ligand. For the most part, in keeping with the theme of Chapter 2, it was logical to continue coordinating N–donor ligands to the Cr(III) centre. As well as the para-substituted pyridine ligands, CH_3CN was also coordinated. Straying slightly from the N-donor trend, the coordination of water was also found to provide important results.

The choice of all the above-mentioned ligands was in keeping with the known donor atoms that have been previously coordinated to Cr(III) to yield catalytically active species successfully.

Although the complexes $[CrCl_3(bipy)(thf)]$ **(9)**, $[CrCl_3(bipy)(CH_3CN)]$ **(10)** and $[CrCl_3(bipy)(py)]$ **(11),** all of which were prepared and characterised in this study, are known complexes [79, 103], their reported synthetic routes differ from those in this study and their

characterisation lacks the detailed spectroscopic data and novel computational data provided here. The reported procedures for making these complexes involve the use of hydrated chromium chlorides, different precursors and solvents.

3.2 SYNTHESIS

Adding the bipyridine to the $[CrCl_3(thf)_3]$ (which had been dissolved in thf) afforded no immediate colour change or formation of precipitate. Over a period of approx. 2 hours the reaction solution turned from deep purple to grey/brown to grey/blue to the final colour of dark green. Once the precipitate had been washed with ether and dried under reduced pressure, a light green precipitate remained.

Owing to the fact that the secondary monodentate ligands (namely the pyridine ligands Chapter 2) coordinated at a much greater speed than the bidentate bipyridine and the fact that the $[CrCl_3(bipy)(thf)]$ compound was virtually insoluble in all solvents, the monodentate ligands were added in one of two ways:

1. $[CrCl_3(bipy)(thf)]$ was resynthesised for each new desired compound and as the green precipitate began to form, the secondary ligand was added.
2. In some cases the $[CrCl_3(bipy)(thf)]$ was soluble in the monodentate ligand and so these ligands were used as both solvent and ligand for the reactions.

3.3 SYNTHETIC ROUTE TO PRODUCT FORMATION

Once all the complexes had been synthesised, there were two key focus areas, namely the characterisation of the complexes and the determination of their synthetic pathways. These areas actually go hand in hand as both rely on the spectroscopic and structural data as tools for characterisation and analysis. The need for confirmation of compound formation is obvious. However, the pathway taken is not a straightforward case of direct ligand substitution as was illustrated in Chapter 2 with the complex $[Hpy][CrCl_4(py)_2]$. The cornerstone of information on which this study was built was the three very different crystal structures that were solved. The first was the neutral monomeric species $[CrCl_3(bipy)(H_2O)]$ **(16)**, the second was the anionic species $[HpyNH_2][CrCl_4(bipy)]$ **(15)** and the third was $[CrCl_2(bipy)_2][Cl]\cdot H_2O$ **(17)**. It is worth mentioning that with respect to $[CrCl_3(bipy)(H_2O)]$, spectra were taken of both the single crystal

material and the precipitate. The fact that these spectra are identical infers that the single crystal determination id representative of the bulk material. Apart from the respective secondary ligands, the method of synthesis for each was unchanged. This clearly leads one to believe that this class of compounds coordinates via the same potential pathways as the monodentate N–ligands.

3.4 INFRARED AND RAMAN SPECTROSCOPY

The key to a successful and comprehensive study of the vibrational spectra of these compounds lies not just in the interpretation of the spectra, but also in the comparative studies that can be undertaken with the results of the other techniques, not to mention the spectra of the other classes of compound. In particular, although there is much overlap in the bands assigned to bipyridine and pyridine, detailed analysis involving comparative studies with the compounds of Chapter 2 can clear up the ambiguity surrounding a number of these bands and in this way they can be assigned specifically to either the bipyridine or pyridine ligands. With regard to band assignment it is perhaps, above all, the comparisons with the spectra of those compounds for which single crystals were obtained that adds the most weight and thus confidence to the assignments. In addition to the presence of the respective ligand vibrations, it is the bands that have shifted to higher frequencies from the free ligand positions that are of particular interest since coordination to the metal is thus implied.

As both IR and Raman spectra of the compound $[HpyNH_2][CrCl_4(bipy)]$ were obtained, comparisons can be made with the other compounds as this will help to deduce whether the final compounds are monomeric or have in fact been cleaved asymmetrically to yield the anionic chromium–pyridinium species. According to the literature [93], important indications will be the strength of bands, as well as their presence or absence, particularly bands indicative of the pyridinium ion. These ions also have a tendency to show greater shifting of bands compared with their neutral counterparts as they possess more prominent polar and conjugation effects [104].

With regard to the results of the individual compounds, it should be noted that Raman spectra were not obtained for the compounds $[CrCl_3(bipy)(pyNH_2)]$ **(12)**, $[CrCl_3(bipy)(H_2O)]$ and $[CrCl_2(bipy)_2][Cl]\cdot H_2O$ owing to problems of fluorescence (see Chapter 1) and lack of sample in the latter case. For the same reason of sample deficiency no FIR spectrum of

$[CrCl_2(bipy)_2][Cl]\cdot H_2O$ was obtained. Note also that the isolated crystal structure, $[HpyNH_2][CrCl_4(bipy)]$, encapsulated a molecule of solvent, namely DCM. Evaporation would explain the lack of evidence of such a molecule in the corresponding IR or Raman spectra.

3.4.1 Region 3329–2291 cm^{-1}

The only complexes to exhibit bands above 3136 cm^{-1} are $[CrCl_3(bipy)(pyNH_2)]$, $[HpyNH_2][CrCl_4(bipy)]$ and $[CrCl_3(bipy)(H_2O)]$ (see Figure 3.1). Both $[CrCl_3(bipy)(pyNH_2)]$ and $[HpyNH_2][CrCl_4(bipy)]$ possess strong IR bands at 3319 and 3312 cm^{-1}, 3206 and 3211 cm^{-1}, as well as 3146 and 3153 cm^{-1} respectively which are indicative of N–H stretching vibrations [96]. $[HpyNH_2][CrCl_4(bipy)]$, in addition, possesses a further three vibrations that are absent in $[CrCl_3(bipy)(pyNH_2)]$. This is an early indication that they are not the same compound, i.e. the addition of $pyNH_2$ does not necessarily lead to the asymmetrically cleaved species. As the structure of $[HpyNH_2][CrCl_4(bipy)]$ has been solved crystallographically, these additional bands are assumed to be pyridinium-related.

While both complexes possess what would appear to be a free $pyNH_2$ ligand shift from 3300 to 3319 and 3312 cm^{-1} respectively, it is plausible that the $[CrCl_3(bipy)(pyNH_2)]$ band is indicative of coordination, while that of $[HpyNH_2][CrCl_4(bipy)]$ is a pyridinium effect. It is worth mentioning that the regions that follow include yet further evidence to suggest differences between the two compounds, in the form of additional bands in $[HpyNH_2][CrCl_4(bipy)]$ that correspond with literature assignments of pyridinium ions.

The relatively benign red shift in $[CrCl_3(bipy)(pyNH_2)]$ has further importance as it indicates that this ligand coordinates to the metal centre via the endocyclic nitrogen, as opposed to the amine substituent where one would have expected a dramatic red shift of between 150 and 200 cm^{-1} [96].

The single, broad, strong band at 3280 cm^{-1} in $[CrCl_3(bipy)(H_2O)]$ is indicative of coordinated water, i.e. characteristic O–H vibration [76, 105].
Between 3139 and 2960 cm^{-1}, all the complexes possess bands associated with the C–H vibrational modes of bipyridine and pyridine [76]. It is very difficult to differentiate between the

two due to their extreme similarities in this regard. However, this has been achieved with some success in the regions that follow.

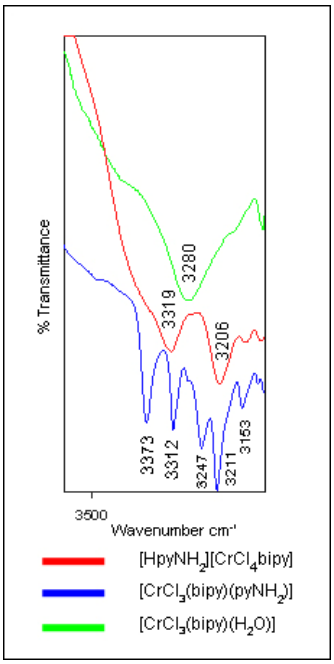

Figure 3.1 IR spectra of [$CrCl_3$(bipy)($pyNH_2$)] (blue), [$HpyNH_2$][$CrCl_4$(bipy)] (red) and [$CrCl_3$(bipy)(H_2O)] (green) in the region 3329 – 2291 cm^{-1}

It is widely recognised that bands indicative of C–H vibrations associated with thf molecules are observed at lower frequencies than those of aromatic molecules [76], and their presence or absence is of importance with respect to the precursor of this study, [$CrCl_3$(thf)$_3$]. The appearance of three such vibrations at 2948, 2929 and 2897 cm^{-1} in [$CrCl_3$(bipy)(thf)] (present as weak vibrations in the equivalent Raman spectrum) suggests that direct ligand substitution, whereby one of the thf molecules remains coordinated to the chromium, is a valid pathway to compound formation. These bands are absent in all the other compounds except for [$CrCl_3$(bipy)(pyphenyl)] **(14),** which may appear to be indicative of a mixture, however, the FAB-MS results presented later suggest otherwise. Figure 3.2 shows the presence of C-H vibrations in [$CrCl_3$(bipy)(thf)] and their absence in [$CrCl_3$(bipy)(H_2O)] while Figure 3.3 compares the spectra of [$CrCl_3$(thf)$_3$] and [$CrCl_3$(bipy)(pyphenyl)].

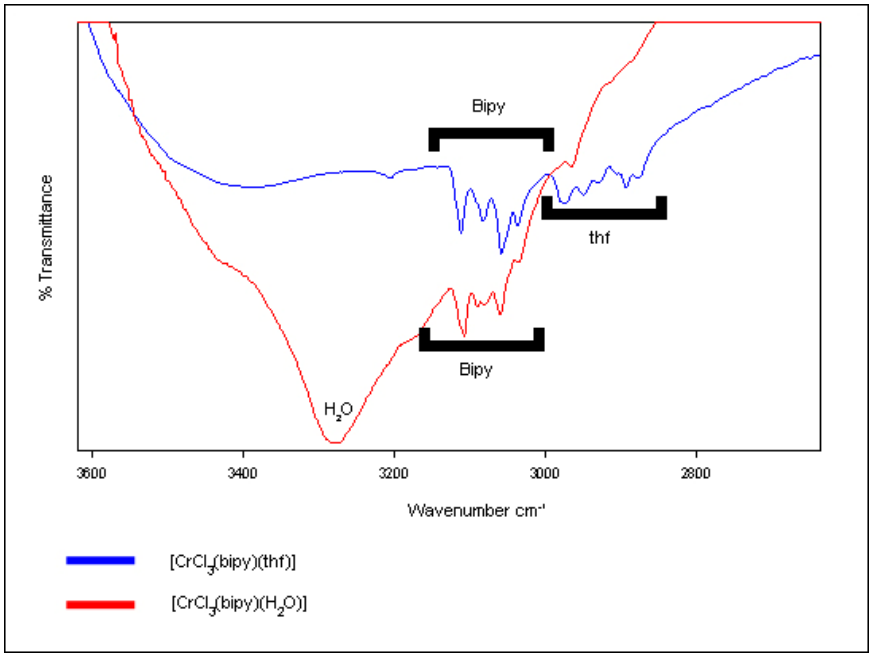

Figure 3.2 **IR spectra showing the presence of thf C–Hs in [$CrCl_3$(bipy)(thf)] (blue) and their absence in [$CrCl_3$(bipy)(H_2O)] (red)**

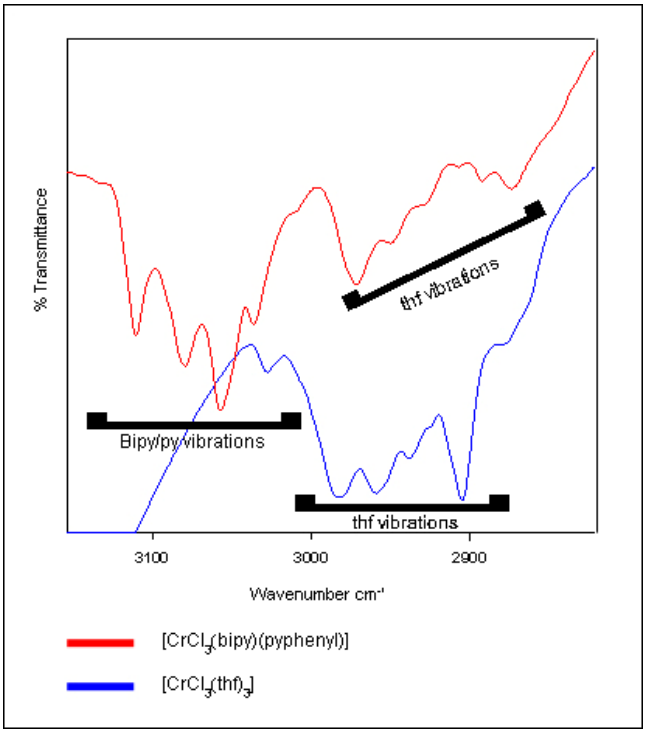

Figure 3.3 **Comparison of the IR spectra of [$CrCl_3$(thf)$_3$] (blue) and [$CrCl_3$(bipy)(pyphenyl)] (red)**

Note that this is really only an early indication as with this information alone it is very difficult to differentiate between coordinated and free thf. The study of coordinated thf is discussed further and with more confidence in the region 1104 to 522 cm^{-1} where more distinctive and conclusive bands are found.

Other bands in this overall region are those associated with the symmetrical and asymmetrical CH_3 stretch vibrations of the tertiary butyl substituent of pytb found in $[CrCl_3(bipy)(pytb)]$ **(13)** (2962 cm^{-1} IR / 2969 cm^{-1} R), (2905 cm^{-1} IR / 2906 cm^{-1} R) and (2868 cm^{-1} IR / 2870 cm^{-1} R) respectively, as well as with the CH_3 symmetrical stretch and C≡N modes of the CH_3CN ligand (2910 cm^{-1} IR / 2913 cm^{-1} R), (2318 cm^{-1} IR / 2321 cm^{-1} R) and (2291 cm^{-1} IR / 2293 cm^{-1} R) respectively. They are all observed as strong vibrations, where R indicates the Raman frequencies. The lack of shifting of the tertiary butyl modes is expected even upon coordination [92], while the CH_3CN modes undergo significant shifts relative to their free ligand positions of 2900 [92], 2289 and 2252 cm^{-1} respectively [79]. Figure 3.4 presents the spectral comparisons between $[CrCl_3(bipy)(CH_3CN)]$ and $[CrCl_3(bipy)(pytb)]$.

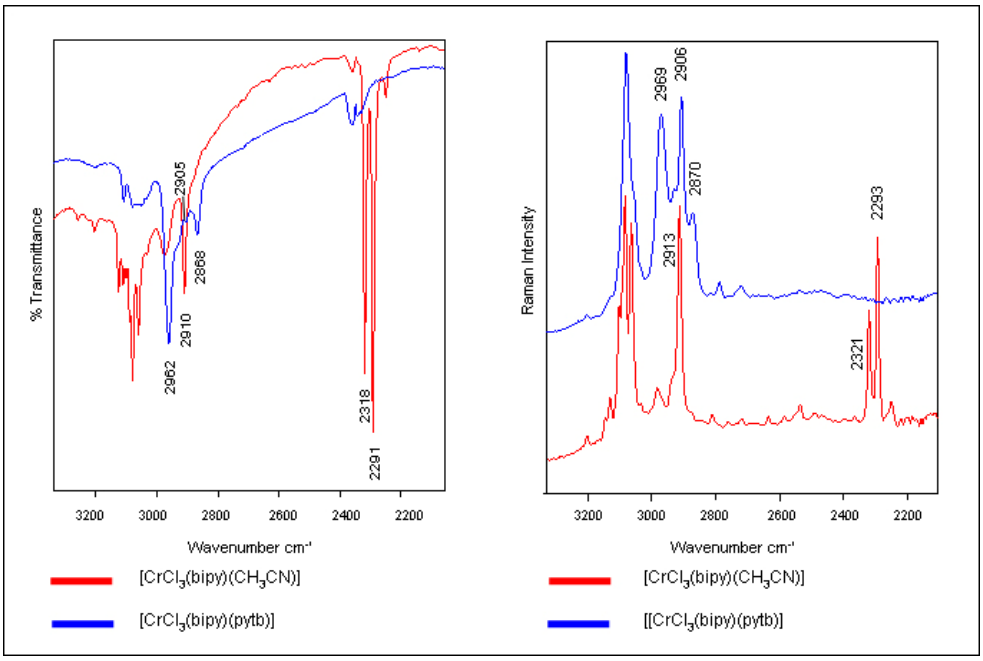

Figure 3.4 **Characteristic IR and Raman vibrations in $[CrCl_3(bipy)(CH_3CN)]$ (red) and $[CrCl_3(bipy)(pytb)]$ (blue)**

3.4.2 Region 1652–1104 cm^{-1}

This particular region possesses bands indicative of both bipyridine and pyridine ring vibrations. These include vibrations that are specifically assigned to the para–substituted pyridine substituents. In addition, pyridinium-specific vibrations associated with ring stretching, C–H bending and N^+-H are also expected. As already stated, one must expect a certain amount of band superposition when investigating compounds involving both bipyridine and pyridine. One such example is the ring vibrations observed at 1596 and 1580 cm^{-1} in free pyridine and also at 1580 cm^{-1} in free bipyridine. Upon coordination all three are expected to shift to ~1600 cm^{-1}, which therefore makes differentiating between the ligands very difficult. Attempts were made, however, by comparing the spectra of the non–pyridine compounds ($[CrCl_3(bipy)(thf)]$, $[CrCl_3(bipy)(H_2O)]$ and $[CrCl_3(bipy)(CH_3CN)]$) and those that do possesses pyridine and its derivatives. Although still no specific assignment to either bipyridine or pyridine could be made, none of the complex spectra showed the free ligand vibrations, which implies that both ligands have coordinated and thus shifted to the higher frequency. Interestingly, a look at the IR spectrum of the $[HpyNH_2][CrCl_4(bipy)]$ complex indicates that the free pyridine vibration at 1580 cm^{-1} has shifted to 1585 cm^{-1} which, in the light of both the above analysis and the confirmed structure of $[HpyNH_2][CrCl_4(bipy)]$, is a pyridinium ion effect. The fact that it is only found in this particular compound suggests that the other compounds are of a neutral, monomeric nature. Note that the same band is absent in the corresponding Raman spectrum.

Figure 3.5 shows the IR comparison of free bipyridine and pyridine with selected spectra representing both the non–pyridine and pyridine compounds, as well as the pyridinium compound. Visible in both figures is another bipyridine band shift from 1556 to 1565 cm^{-1} upon coordination, with band splitting evident in the IR spectrum.

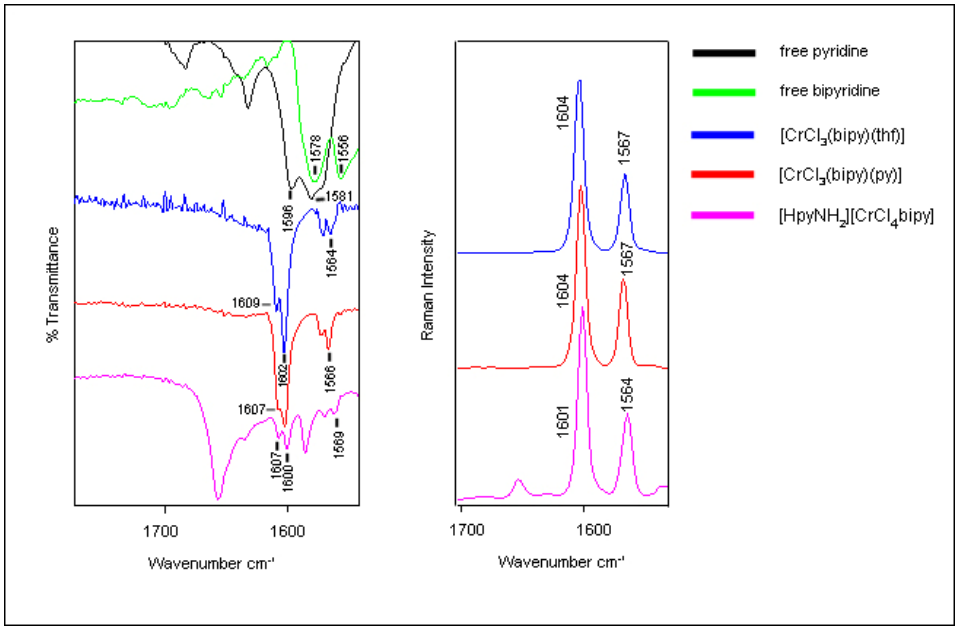

Figure 3.5 **IR and Raman vibrations in [$CrCl_3$(bipy)(thf)] (blue), [$CrCl_3$(bipy)(py)] (red) and [$HpyNH_2$][$CrCl_4$(bipy)] (purple)**

There are a number of other vibrations that are either bipyridine or pyridine-specific. Table 3.1 highlights the bipyridine ring vibrations (as well as a CN mode at 1318 cm^{-1}) that are absent in the pyridine literature [73, 74]. Figure 3.6 compares the IR spectra of [$CrCl_3$(bipy)(thf)] and [$CrCl_3(py)_3$].

Table 3.1 **Bipyridine-specific vibrations present in the spectra of all complexes**

Free bipy / cm^{-1}	Bipy complexes / cm^{-1}	Shift / cm^{-1}
1557	1564	7
1496	1496	0
1472	1472	0
1318	1318	0
1245	1245	0
1090	1104	14

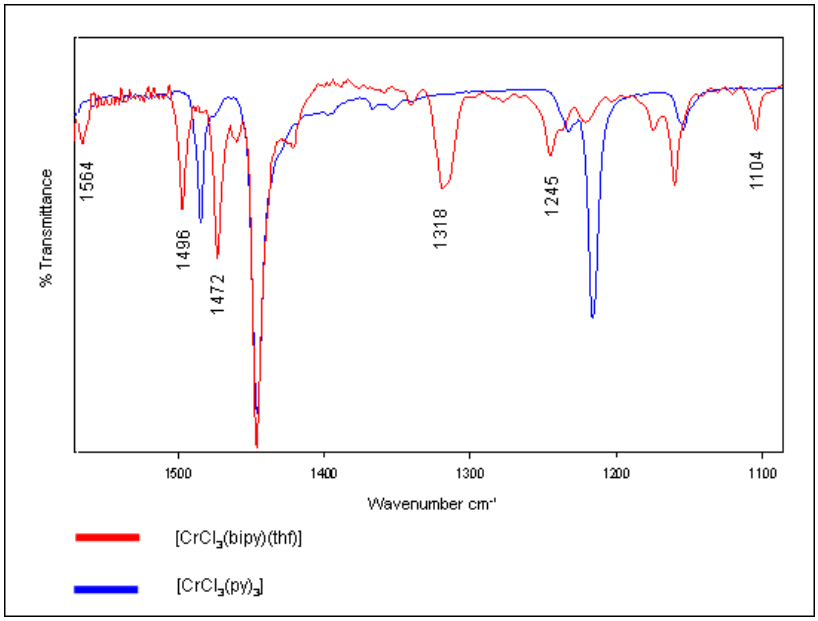

Figure 3.6 **Bipyridine specific IR vibrations present in all complexes represented by the comparison between [$CrCl_3$(bipy)(thf)] (red) and [$CrCl_3(py)_3$] (blue)**

The pyridine ring vibrations are largely influenced by their substituents, hence there is no band superposition observed (see Table 3.2).

Table 3.2 **Pyridine specific vibrations**

	Free ligand / cm^{-1}	Complex / cm^{-1}	Shift / cm^{-1}
$pyNH_2$	1506	1530	14
	-	1196	-
pytb	-	1397	-
pyphenyl	1512	1513	1
	1279	1291	12

The only substituent vibrations that are visible are those associated with the tertiary butyl group and these appear to be unshifted, which correlates to similar metal-coordinated compounds in the literature. They are observed at (1365 cm^{-1} IR / 1360 cm^{-1} R), (1202 cm^{-1} IR / 1203 cm^{-1} R) and (1120 cm^{-1} IR / 1128 cm^{-1} R); the first is assigned to a CH_3 asymmetrical deformation while the other two are C=C stretches [92]. See Figure 3.7.

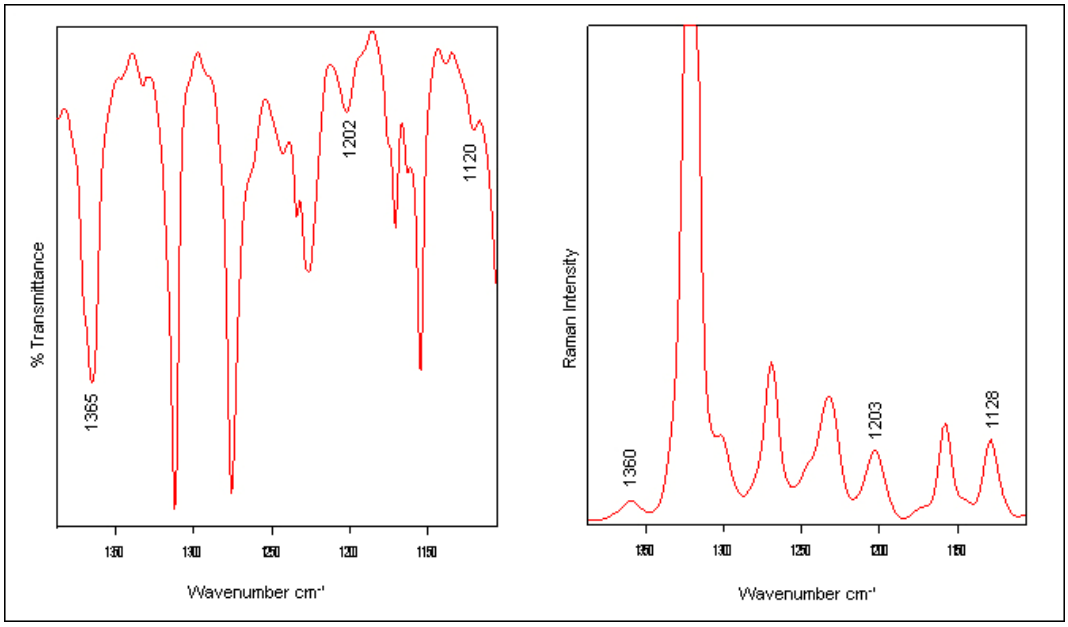

Figure 3.7 IR and Raman vibrations of tertiary butyl-specific vibrations in the region 1652 – 1104 cm^{-1}

3.4.3 Region 1104–522 cm^{-1}

This is an important region not just because there is further evidence of ligand coordination by way of free-ligand vibrational shifts, but also because of the ability to discuss some of these shifts with regard to bond strength. As this is common to Chapter 2, both experimental comparisons and literature comparisons can be made.

Evidence of coordinated thf is also visible, which helps to shed light on the synthetic route to compound formation. In the same vein, further comparisons with the spectrum of $[HpyNH_2][CrCl_4(bipy)]$ are helpful and, as expected, there are also a number of pyridine substituent vibrations.

Due to the band superposition already discussed, some of the vibrations that could equally be assigned to bipyridine or pyridine are those at ~1070, ~1060, ~1032 and ~769 cm^{-1}. Little to no shifting is observed upon complexation, except in the case of 769 cm^{-1} (shifted from 756 cm^{-1} in bipyridine or 749 cm^{-1} in pyridine).

3.4.3.1 Pyridine-specific

In the light of the vibrational assignments in Chapter 2, much emphasis is placed on the free-pyridine ring breathing mode found at ~992 cm^{-1} which shifts relative to the substituents. A number of factors are responsible for the extent of shifting, including mass, number, nature and position of substituents [75].

Interestingly, the degrees of shifting of all the ligand-specific vibrations in all the complexes correspond very well to those of Chapter 2 (see Table 3.3 and Figure 3.8) and seem unaffected by the change of complex environment (i.e. coordinated bipyridine). With regard to $pyNH_2$, this shift is yet further evidence of endocyclic nitrogen coordination as opposed to the equally plausible amino group coordination.

Table 3.3 Shifting of the characteristic ring breathing vibration in $[CrCl_3(bipy)(py)]$, $[CrCl_3(bipy)(pyNH_2)]$, $[CrCl_3(bipy)(pytb)]$ and $[CrCl_3(bipy)(pyphenyl)]$

Pyridine / cm^{-1}	$[CrCl_3(bipy)(py)]$ / cm^{-1}	Shift / cm^{-1}
990	1013	23

$pyNH_2$ / cm^{-1}	$[CrCl_3(bipy)(pyNH_2)]$ / cm^{-1}	Shift / cm^{-1}
991	1022	31

Pytb / cm^{-1}	$[CrCl_3(bipy)(pytb)]$ / cm^{-1}	Shift / cm^{-1}
995	1025	30

Pyphenyl / cm^{-1}	$[CrCl_3(bipy)(pyphenyl)]$ / cm^{-1}	Shift / cm^{-1}
1001	1011	10

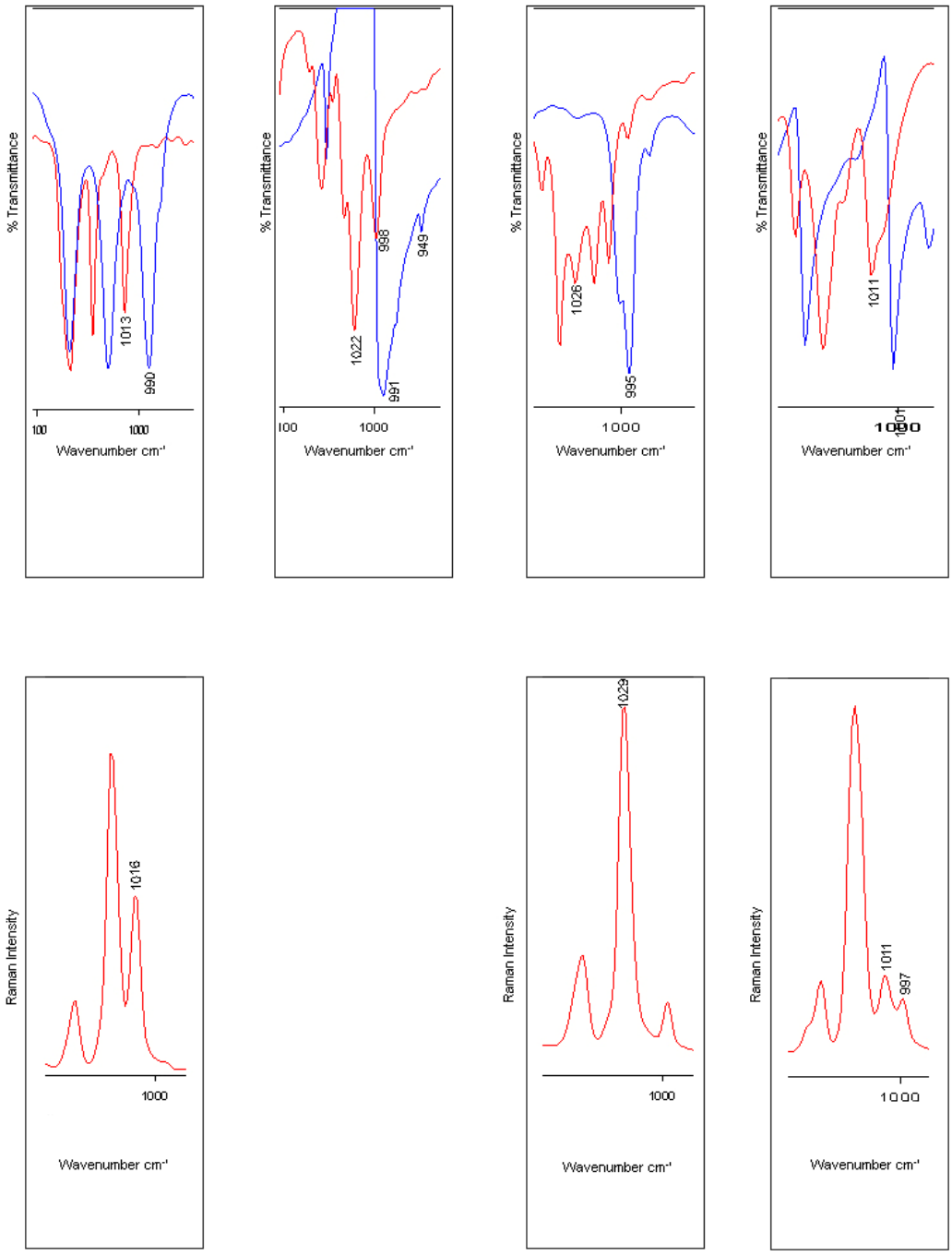

Figure 3.8 **Spectra showing the shifting of the characteristic ring breathing vibration in the IR of [$CrCl_3$(bipy)(py)], [$CrCl_3$(bipy)($pyNH_2$)], [$CrCl_3$(bipy)(pytb)] and [$CrCl_3$(bipy)(pyphenyl)] from free ligand positions. Raman spectra of [$CrCl_3$(bipy)(py)], [$CrCl_3$(bipy)(pytb)] and [$CrCl_3$(bipy)(pyphenyl)]**

Although pytb shows a second band at 1015 cm^{-1}, it is the band at 1026 cm^{-1} that corresponds with the shift observed for the similar complex, $[CrCl_3(pytb)_3]$, in Chapter 2. Indeed, in the chapters that follow the same band at 1026 cm^{-1} is also exhibited upon addition of the pytb ligand.

The presence of a band at 1022 cm^{-1} in $[HpyNH_2][CrCl_4(bipy)]$ is assignable to a pyridinium α(C–C–C) vibration [94, 95].

Another pyridine vibration that characteristically shifts upon coordination is that at 605 cm^{-1} [73, 74], which is found in the complexes at 643 cm^{-1} (see Figure 3.9). Even though it is also present in $[HpyNH_2][CrCl_4(bipy)]$, one must expect vibrational overlap and it is more than likely a pyridinium-type band. Although unshifted, a further pyridine vibration is that observed at 698 cm^{-1} [97].

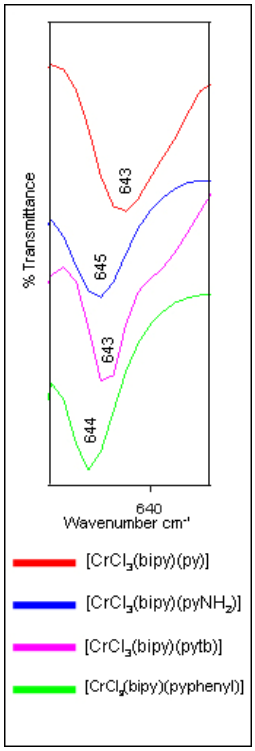

Figure 3.9 **Evidence of coordinated pyridine in the IR spectra of $[CrCl_3(bipy)(py)]$ (red), $[CrCl_3(bipy)(pyNH_2)]$ (blue), $[CrCl_3(bipy)(pytb)]$ (purple) and $[CrCl_3(bipy)(pyphenyl)]$ (green)**

There are also a number of vibrations associated with the respective pyridine substituents. The tertiary butyl bands at 930 (CH_3 rock) and 661 cm^{-1} (C–C stretch) follow the trend of similar compounds in the literature by not undergoing shifting upon coordination [92], while the lone phenyl ring mode observed at (625 cm^{-1} IR / 616 cm^{-1} R) also follows the literature and does shift from 608 cm^{-1} [97]. Amino vibrations are observed in both [$CrCl_3$(bipy)($pyNH_2$)] and [$HpyNH_2$][$CrCl_4$(bipy)] at 855 (X-sens), 527 cm^{-1} (X-sens) [96]. They undergo coordinative shifts from 842 and 522 cm^{-1} respectively. A further band at 501 cm^{-1} is not observed in the literature but is observed only in these two compounds and is thus assigned to a $pyNH_2$ vibration.

3.4.3.2 Bipyridine-specific

With regard to bipyridine-exclusive bands, it would appear that only those at ~995, 730, 665 and 651 cm^{-1} are assignable. 730 cm^{-1} is not present in free bipyridine nor in any of the other ligands and its presence is therefore assumed to be a coordination indicator, perhaps associated with the formation of the chelate ring.

3.4.3.3 Thf-specific

One of the most important assignments within this region elucidates the synthetic pathway via which these compounds are formed. Strong IR bands at 1006 and 856 cm^{-1} are indicative of coordinated thf [77, 78] and both of these vibrations are found in [$CrCl_3$(bipy)(thf)] (note that in the equivalent Raman spectrum the 1006 cm^{-1} mode is absent and that at 856 cm^{-1} is very weak). This is strong evidence to suggest that direct ligand substitution is a plausible route of synthesis resulting in the monomeric species and builds on the evidence observed in the region 3329–2291 cm^{-1}. There is a band similar to that at 1006 cm^{-1} in [$CrCl_3$(bipy)(pytb)] and [$HpyNH_2$][$CrCl_4$(bipy)]. As the crystal structure of the latter has been solved, and no thf is present, it can be assigned to a pyridinium vibration. Unlike the thf mode, this vibration is clearly visible in the equivalent Raman spectrum. Figure 3.10 shows the IR and Raman spectra of the above compounds.

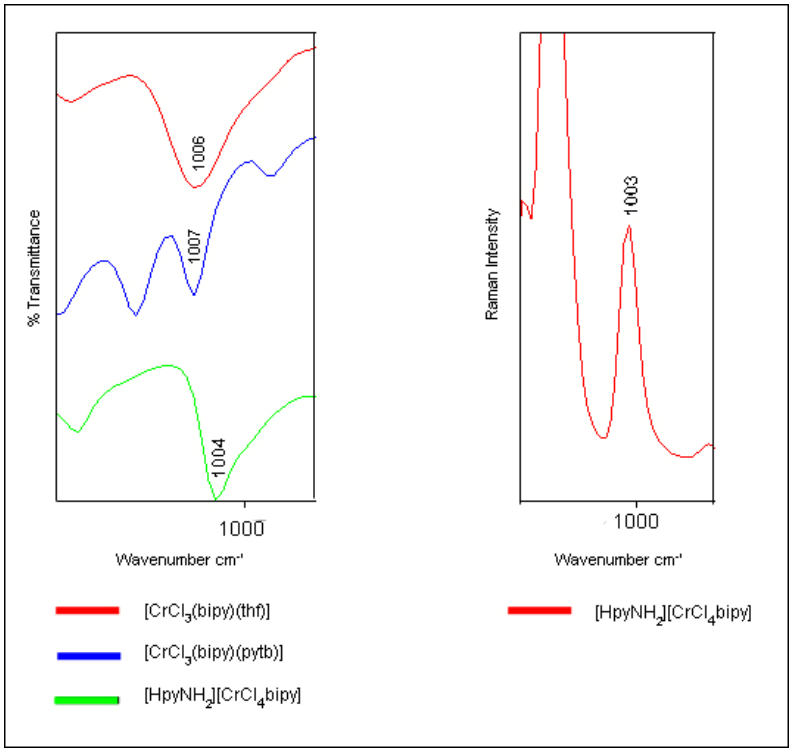

Figure 3.10 **Thf / unassigned / pyridinium vibration in IR and Raman spectra of [$CrCl_3$(bipy)(thf)] (red), [$CrCl_3$(bipy)(pytb)] (blue) and[$HpyNH_2$][$CrCl_4$(bipy)] (green)**

Regarding the 856 cm^{-1} vibration, it is also observed in [$CrCl_3$(bipy)($pyNH_2$)] (prominent shoulder), [$HpyNH_2$][$CrCl_4$(bipy)] and [$CrCl_3$(bipy)(pyphenyl)]. Its presence in the two amino compounds can be explained as a $pyNH_2$ vibration according to the literature [96, 98], but its unexpected presence in [$CrCl_3$(bipy)(pyphenyl)] may be an indication of a mixture of substituted and unsubstituted material, once again backed by the C–H (thf) bands in the region 3329–2291 cm^{-1}. In the same mould as the 1006 cm^{-1} mode, only the [$HpyNH_2$][$CrCl_4$(bipy)] Raman spectrum showed a band of worthwhile intensity. The IR spectra of [$CrCl_3$(bipy)(thf)], [$CrCl_3$(bipy)($pyNH_2$)], [$CrCl_3$(bipy)(pyphenyl)] and [$HpyNH_2$][$CrCl_4$(bipy)] in addition to the Raman spectrum of [$HpyNH_2$][$CrCl_4$(bipy)] are presented in Figure 3.11.

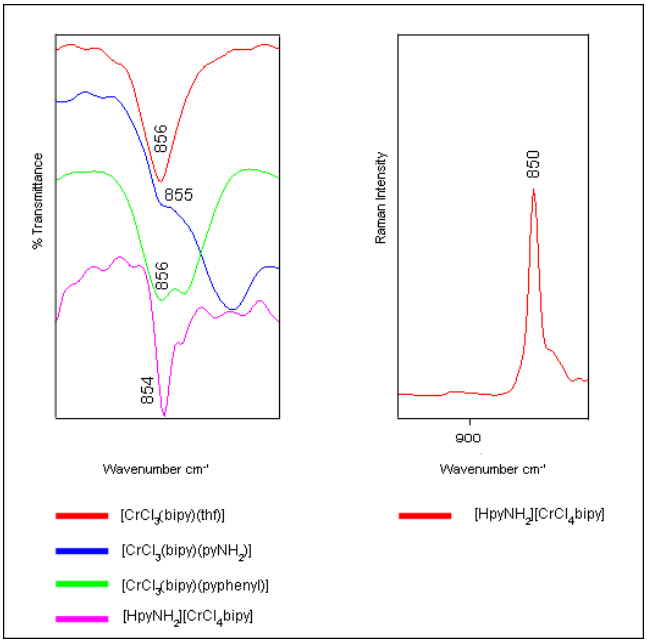

Figure 3.11 IR spectrum of [$CrCl_3$(bipy)(thf)] (red), [$CrCl_3$(bipy)($pyNH_2$)] (blue), [$CrCl_3$(bipy)(pyphenyl)] (green) and[$HpyNH_2$][$CrCl_4$(bipy)] (purple). Raman spectrum of [$HpyNH_2$][$CrCl_4$(bipy)]

.

3.4.3.4 Pyridinium-specific

Throughout the above discussions pyridinium-assignable vibrations have already been mentioned (1022, 1004 and 643 cm^{-1}). In addition, there are a further two modes that are present solely in [$HpyNH_2$][$CrCl_4$(bipy)] and are observed at 1046 and 590 cm^{-1}. Both are yet further evidence of monomeric product formation with respect to the other compounds. See Figure 3.12.

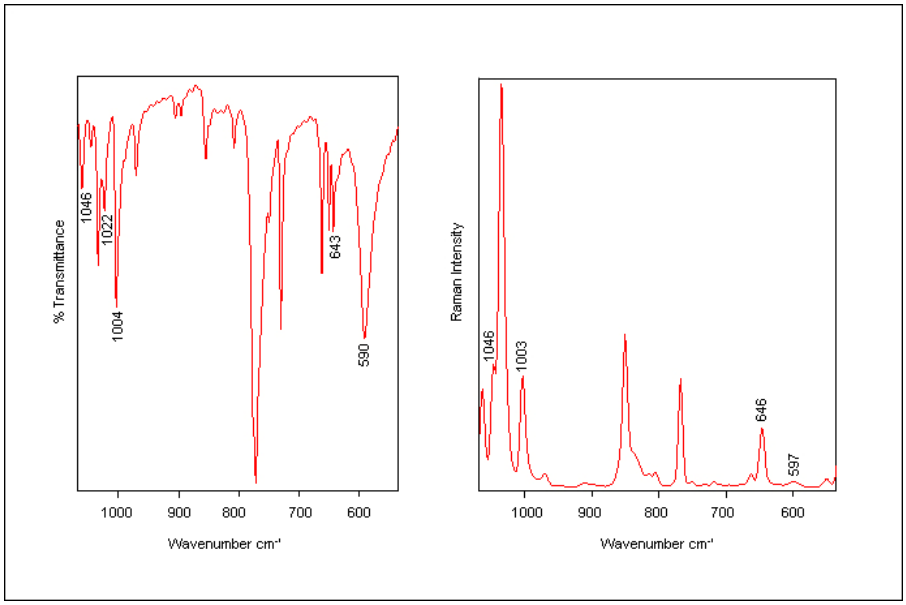

Figure 3.12 **IR and Raman bands associated with [HpyNH$_2$][CrCl$_4$(bipy)]**

3.4.4 Region 451–221 cm^{-1}

As can be seen in Table 3.4, the vibrations discussed here are present in both the IR and Raman spectra. However, the intensity of many of the Raman vibrations is a lot weaker than that of their IR counterparts. For this reason the representative spectra shown in Figure 3.13 are IR vibrations.

This is perhaps the most important region with regard to ligand coordination, and indeed compound geometry, as the bands are associated predominantly with metal–ligand vibrations. There is, however, a small number of pure ligand modes; the emphasis is on the word 'small' as their scarcity in this region is advantageous since the ambiguity that comes with band overlap as in the other regions is ruled out. The modes include bands at 428 and 402 cm^{-1} in free bipyridine which characteristically shift upon coordination to values of ~451 and ~414 cm^{-1} respectively [79]. These are common to all the compounds. The lone pyridine vibration is observed at 405 cm^{-1} and its shifting to around 442 cm^{-1} is widely accepted to be indicative of coordination [73, 74]. Note that it is solely observed in the unsubstituted pyridine compound, which is identical to what was observed in the previous chapter.

The geometry of the compounds can be linked to the number of Cr–Cl vibrations observed. The presence of two Cr–Cl bands indicates the *cis* isomer, while three Cr–Cl bands imply that the *mer* isomer has been adopted [80]. As per the crystal structure of the monomer $[CrCl_3(bipy)(H_2O)]$, whereby the *mer* configuration is adopted, three bands are visible for nearly all the compounds. In the case of $[HpyNH_2][CrCl_4(bipy)]$, which is an asymmetrically cleaved dimer, four strong Cr–Cl bands are observed and this is in agreement with literature findings on similar compounds [99].

The ability to assign specific M–N bonds is of obvious interest and indeed importance. The Cr–N bands associated with the coordination of bipyridine and pyridine are seen in the spectra between 236 and 246, and at 221 cm^{-1} respectively [41, 79, 80, 81]. The band at 209 cm^{-1} in $[CrCl_3(bipy)(pyphenyl)]$ falls outside the assigned range, but can be explained by the fact that increasing the mass of the ring by substitution lowers the metal–N value [81]. Also the 222 cm^{-1} vibration in $[HpyNH_2][CrCl_4(bipy)]$ is related to a pyH mode.

The tentative assignment of the Cr–O (thf) band at 284 cm^{-1} is based on work by Fowles [82]. The same band has also previously been assigned to other vibrations, including the skeletal stretch of H_2O [106]. It is interesting to note that this band with a slight downward shift is present in all the complexes except $[CrCl_3(bipy)(pyphenyl)]$. As this includes the known structural identity of $[HpyNH_2][CrCl_4(bipy)]$, one must assume that it is also assignable to a bipyridine/pyridine vibration common to all.

As in previous work, the assignment of Cr–N (CH_3CN) has not been made [107]. It is also notable that no Cr–O (H_2O) bands in $[CrCl_3(bipy)(H_2O)]$ are present where expected, although the crystal structure along with other IR bands (presence of sharp water band and absence of coordinated thf) suggests otherwise.
Figure 3.13 is a representation of what is seen in all the spectra with regard to:

- The absence of the unsubstituted pyridine mode that is observed solely in $[CrCl_3bipy(py)]$ at 442 cm^{-1}
- The presence of the two shifted bipyridine vibrations at ~451 and ~414 cm^{-1} respectively

- The three Cr–Cl vibrations common to all complexes except [$HpyNH_2$][$CrCl_4$(bipy)], which exhibits four
- The Cr–N (bipy) between 236 and 246 cm^{-1} and the Cr–N (py) at ~221 cm^{-1}.

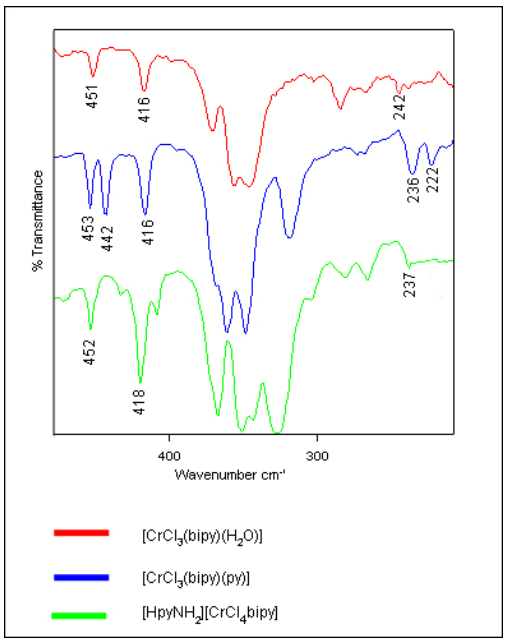

Figure 3.13 **FIR vibrations represented by spectra of [$CrCl_3$(bipy)(H_2O)] (red), [$CrCl_3$(bipy)(py)] (blue) and [$HpyNH_2$][$CrCl_4$(bipy)] (green)**

Table 3.4 Vibrational assignments of $[CrCl_3(bipy)(thf)]$ (9), $[CrCl_3(bipy)(CH_3CN)]$ (10), $[CrCl_3(bipy)(py)]$ (11), $[CrCl_3(bipy)(pyNH_2)]$ (12), $[CrCl_3(bipy)(pytb)]$ (13), $[CrCl_3(bipy)(pyphenyl)]$ (14), $[HpyNH_2][CrCl_4(bipy)]$ (15), $[CrCl_3(bipy)(H_2O)]$ (16) and $[CrCl_2(bipy)_2][Cl]\cdot H_2O$ (17)

9		10		11		12	13		14		15		16	17	assignment
IR / cm^{-1}	R / cm^{-1}	IR / cm^{-1}	R / cm^{-1}	IR / cm^{-1}	R / cm^{-1}	IR / cm^{-1}	IR / cm^{-1}	R / cm^{-1}	IR / cm^{-1}	R / cm^{-1}	IR / cm^{-1}	R / cm^{-1}	IR / cm^{-1}	IR / cm^{-1}	
-	-	-	-	-	-	-	-	-	-	-	3373s	3376w	-	-	ν (NH_2) (96)
-	-	-	-	-	-	3319s	-	-	-	-	3312s	3313w	-	-	ν (NH_2) asym (76, 96)
-	-	-	-	-	-	-	-	-	-	-	-	-	3280s	-	ν(OH) (76, 105)
-	-	-	-	-	-	-	-	-	-	-	3278w	3275w	-	-	ν (NH_2) (96)/ pyH
-	-	-	-	-	-	-	-	-	-	-	3247s	3244w	-	-	ν (NH_2) (96)/ pyH
-	-	-	-	-	-	3206s	-	-	-	-	3211s	3214w	-	-	ν (NH_2) sym (76, 96)
-	-	-	-	-	-	3146s	-	-	-	-	3153s	3142w	-	-	ν (NH_2) sym (76, 96)
-	3132w	3126m	3129w	3136vw	3139w	-	-	3126w	-	3132w	3119s	3127w	-	-	Bipy/py ν(CH) (73, 74, 76)
3107s	-	3107m	3101m	3107m	-	3111s	3109m	-	3110s	-	3104s	3104w	3106s	3112m	Bipy/py

9		10		11		12	13		14		15		16	17	assignment
															ν(CH) (73, 74, 76)
3081s	3079s	3080m	3082m	3083m	3088s	3088s	3080m	3079s	3080s	3085m	3080s	3077s	3089s 3078s	3084m 3075m	Bipy/py ν(CH) (73, 74, 76)
3057s	3062m	3061m	3064m	3063m	3065m	3060sh	3068m 3066m	-	3057s	3064sh	3060s 3053s	3071s 3056w	3059s	3060w	Bipy/py ν(CH) (73, 74, 76)
-	-	-	-	3048m	3052m	-	3056m	3056sh	-	-	-	-	-	3052w	Bipy/py ν(CH) (73, 74, 76)
3036s	3037w	-	-	-	-	3036sh	3034m	3034sh	3036s	-	3032s	3033w	3034s	3027w	Bipy/py ν(CH) (73, 74, 76)
2979s	2982w	2966m	2987w	2973m	2960w	2969s	-	-	2971m	2985vw	2972s	2979w	2964sh	2976w	Bipy/py ν(CH) (73, 74, 76)
-	-	-	-	-	-	-	2962s	2969s	-	-	-	-	-	-	ν (CH_3) asym (tb) (92)
2948s 2929s	2948vw 2932w	-	-	-	-	-	-	-	2948m	2949vw	-	-	-	-	thf ν(CH) (76)
-	-	-	-	-	-	-	2927m	2928m	-	-	-	-	-	-	ν (CH_3) sym (tb) (92)

9		10		11		12	13		14		15		16	17	assignment
-	-	2910m	2913s	-	-	-	2905m	2906s	-	-	-	-	-	-	ν (CH_3) sym (MeCN) / (pytb) (92)
2897s	Nv	-	-	-	-	-	-	-	2892m	2892vw	-	-	-	-	thf -ν(CH) (76)
2876m	2873w	-	-	-	-	-	-	-	2874m	2874vw	-	-	-	2875w	unassigned
-	-	-	-	-	-	-	2868m	2870m	-	-	-	-	-	-	ν (CH_3) sym (tb) (92)
-	-	2318m	2321m	-	-	-	-	-	-	-	-	-	-	-	δ(CH_3) sym + ν(CC) – MeCN (79)
-	--	2291m	2293m	-	-		-	-	-	-	-	-	-	-	ν(C≡N) (79)
-	-	-	-	-	-	1651s	-	-	-	-	1656s	1653m	-	-	δ(NH_2) (96)
-	-	-	-	-	-	-	-	-	-	-	-	-	1608s	-	H-O-H (105)
1609m	-	1608m	-	1607m sh	-	1610sh	1609s	-	1610s	1613sh	1607m	-	-	-	Coord ν_{ring} (bipy)/(py)/ pyH (73, 74, 104)
1602s	1604s	1600s	1600s	1602s	1604s	1601s	1601s	1602s	1602m	1600vs	1600m	1601s	1600s	1601m	Coord ν_{ring} (bipy) (76)
-	-	-	-	-	-	-	-	-	-	-	1585m	-	-	-	pyH ν(CC)

9		10		11		12	13		14		15		16	17	assignment
-	-	-	-		-	1572w	1572m	-	1572w	-	-	-	-	1578m	ν_{ring} (py) (73-76, 92-97)
1564w	1567s	1564w	1567s	1566w	1567s	1565w	1564m	1564s	1565w	1567s	1569w 1561w	- 1564s	1568w	-	ν_{ring} (bipy) (73, 74, 76)
-	-	-	-	-	-	1555w	1547m	-	-	-	-	-	-	1557m	ν_{ring} (py) (73-76, 92-97)
-	--	-	-	-	-	1528s	-	-	-	-	1530s	1533w	-	-	ν_{ring} ($pyNH_2$) (96)
-	-	-	-	-	-	-	-	-	1513vw	1513vw	-	-	-	-	ν_{ring} (pyphenyl) (97)
1496m	1497s	1494w	1497s	1495w	1497s	1496m	1495m	1498s	1496w	1496s	1495w	1497s	1497m	1497w	ν_{ring} (bipy) (76)
1472s	-	1470m	1469vw	1471w	1473vw	1471m	1471m	1483w	1472m	-	1473m	-	1472m	1470w	ν_{ring} (bipy) (76)
1446s	1440w	1440s	1436w	1445s	1437w	1444s	1445s	1448m	1445s	1440w	1443s	1443w	1445s	1447s	ν_{ring} (bipy/py) (73-76, 92-97)

9		10		11		12	13		14		15		16	17	assignment
1421w	1424w	1418 sh	1419w			1420w	1418m	1421w	1418m	1420w	1426sh	1420w	1422w	1415m	ν_{ring} (bipy/py) (73-76, 92-97)
-	-	-	-	-	-	-	1397sh	1399w	-	-	-	-	-	-	pytb
-	-	1367w	1367w	-	-	-	1365m	1360w	-	-	-	-	-	-	(CH_3) asym def (tb) (92)
1341vw	1352w	-	1350w	1347vw	1345w	1358w	1346m	-	1340vw	1352w	-	-	-	-	ν_{ring} (bipy/py) (73-76, 92-97)
1318m	1321s	1318w 1309m	1317s -	1313m	1321s	1313m	1312m	1320s	1313m	1317s	1319m	1318s	1313m	1315m	ν_{ring}(CN) (76)
-	-	-	-	-	-	-	-	-	1291w	1292s	-	-	-	-	ν_{ring} + δ(CH) (pyphenyl) (97)
1277vw	1271m	-	-	1276vw	-	1284w	1275m	1269m	1280vw	1276m	1283w	1285vw	1281vw	1278w	C-NH_2 / δ(CH) (bipy/py) (73-76, 92-97)
-	-	1261w	1269m	1261w	1268m	1263vw	-	-	-	-	-	1269	1259w	1268w	ν_{ring} (bipy/py) (73-76, 92-

9		10		11		12	13		14		15		16	17	assignment
															97)
1247m	1247w	1242w	1244w	1245w	1246w	1245w	-	-	-	-	1245m	1249m	1242w	1249m	ν_{ring} (bipy) (73-76, 92-97)
1218w	-	1220w	1220vw	1210w	1213w	1216s	1227w	1232m	1225m	-	1220w	1220m	1222w	1212w	δ(CH) (bipy/py) (73-76, 92-97)
-	-	-	-	-	-	-	1202w	1203m	-	-	-	-	-	-	ν (CC) (tb) (92)
-	-	-	-	-	-	1196s	-	-	-	-	1194m	1197w	-	-	$PyNH_2$
-	-	-	-	1175w	1178w	1174m	1163w	-	1173w	-	1174m	1174w	1167w	1177w	ν(CC/CH) (bipy/py) (73-76, 92-97)
1160m	1160m	1165w	1168w	1161w	1163w	1159m	1156m	1157m	1159m	1158w	1157m	1158m	1156m	1160w	ν(CC/CH) (bipy/py) (73-76, 92-97)
-	-	1146w	1151m	-	-	-	-	-	-	-	-	-	-	-	MeCN vib
-	-	1116w	1118vw	-	-	1121vw	1122vw	1128m	-	-	-	1118w	-	-	ν (CC) (tb) (92)
1104w	1104w	1101w	1100w	1106w	1108w	1107w	1107w	1108vw	1105w	1105w	1106w	1107w	1105m	1106w	ν_{ring} (bipy) (76)
-	-	1070w	-	-	-	1072sh	1074m	-	1070m	-	1073w	-	1072m	-	δ (CH)

9		10		11		12	13		14		15		16	17	assignment
															(py/bipy) (73-76, 92-97)
1063w	1062m	-	1064m	1064s	1066m	1058m	1058m	1064m	1062m	1063w	1060w	1063m	1060m	1064w	ν(CC/CH) (bipy/py) (73-76, 92-97)
-	-	-	-	-	-	-	-	-	-	-	1046w	1046m	-	-	pyH ν(CC) (93)
1034m	1035s	1033m	1035s	1035m	1036s	1033m	1034m	-	1033m	1038s	1033m	1035s	1035m	1039m 1031m	ν(CC/CH) (bipy/py) (73-76, 92-97)
-	-	-	-	-	-	-			-	-	1022w	-	-	-	pyH α(CCC) (94, 95)
-	-	-	-	1013w	1016s	1022s	1026m 1015m	1029s -	1011m	1011w		-	-	-	Ring breathing (pyX) (73-75)
1006m	-	-	-	-	-		1007m	-	-	-	1004m	1003m	-	-	Coord thf ν (COC) asym (77, 78) / pyH ν(CC) (95)

9		10		11		12	13		14		15		16	17	assignment
-	-	-	-	-	-	998m	998vw	996m	-	997w	-	-	-	991m	ν_{ring} (bipy) (76) / pyX-specific / ring breath (113)
-	-	-	-	-	-	-	930vw	930w	-	-	-	-	-	-	(CH_3) rock (tb) (92)
856s	854vw	-	-	-	-	855w	-	-	856s	849w	854w	850m	-	-	Coord thf ν (COC) sym (77, 78) / ($pyNH_2$) (96, 98)
-	-	-	-	-	-	-	842w	844w	847s	-	-	-	-	-	Py breathing (92)
-	-	-	-	-	-	830m	827m	-	-	-	-	816w	-	-	δ (CH) py (92, 96)
769s	766m	768s	771m	761s	768s	770s	768s	767m	768vw	768m	771s	768m	779s 772s	-	ν_{ring} / δ_{ring} (bipy/py) (73-76, 92-97)
-	-	-	-	-	-	-		-	750br	750w	-	-	754w	756s	ν_{ring} (bipy) (76)
730s	-	730m	739w	-	-	730s	731m	732m	730s	-	730m	732vw	729s	729m	ν_{ring} (bipy)

9		10		11		12	13		14		15		16	17	assignment
															(76)
-	-	-	-	698s	-	694	-	-	693m	-	-	-	-	-	ν_{ring} (py) (97)
665m	669w	664w	665w	663w	663vw	663m	667m	668m	663m	667w	661m	661vw	663m	665m	ν_{ring} (bipy) (76)
-	-	-	-	-	-	-	661m	-	-	-	-	-	-	-	N(CC) (pytb) (92)
651m	646w	649m	646w	650w	650m	652m	651m	-	-	-	650m	-	650m	654w	ν_{ring} (bipy)
-	-	-	-	643w	-	645m	643m	643w	-	646w	642m	646m	-	-	Coord δ_{ring} (py) / pyH α(CCC) (73, 74)
-	-	-	-	-	-	-	-	-	625m	616w	-	-	-	-	δ_{ring} (pyphenyl) (97)
-	-	-	-	-	-	-	-	-	-	-	590s	597vw	-	-	ν(CC) PyH
-	-	-	-	-	-	572m	568m	-	564m	565w	-	-	-	-	δ_{ring} / skeletal str (tb) (92, 97)
-	-	-	-	-	-	527s	-	-	-	-	528m	529m	-	-	X-sens ($pyNH_2$) (96)
-	-	-	-	-	-	501s	-	-	-	-	498m	501w	-	-	$PyNH_2$
451w	451w	454m	-	453m	470w	453m	451w	452vw	454m	-	452w	452w	451m	450w	Coord bipy ring def

9		10		11		12	13		14		15		16	17	assignment
															(79)
-	-	-	-	442m	442w	-	-	-	-	-	-	-	-	-	Coord py (73, 74)
414m	418br	415m	410w	416m	-	419m	417w	-	419m	424w	418m	420m	416m	416w	Coord ring def (bipy) (79)
369s	369m	365sh	369m	360s	365m	369s	366s	-	372s	369m	366s	367w	371s	-	Cr – Cl (80, 99)
355s	350m	352s	350m	348s	350m	346s	352s	355m	355s	352sh	350s	352m	355s	-	Cr – Cl (80, 99)
345s	341m	337s	336sh	319s	317vw	328ssh	323sbr	335m	323s	304w	343s	-	346s	-	Cr – Cl (80, 99)
-	-	-	-	-	-	-	-	-	-	-	327s	326vw	-	-	Cr – Cl (80, 99)
284w	271s	276w	276s	273vw	271s	279w	282m	-	-	-	280w	-	284w	-	Bip/py/Cr-O (thf)(82)/ Cr-O (H_2O) (106)
-	-	-	-		-	-	274m	-	-	-	-	-	-	-	unassigned
-	-	-	-	-	-	-	266m	267m	267vw	270m	265w	268s	-	-	unassigned
244w	234m	243w	244w	236w	236m	236w	246m	-	236m	232w	237w	235m	242vw	-	Cr – N (bipy) (79)
-	-	-	-	222w	222m	220w	220m	229m 216m	209w	213w	220w	220m	-	-	Cr – N (py) (41, 80, 81)/pyH

ν = stretching, δ = in plane bending, γ = out of plane bending, def = deformation, asym = asymmetric, sym = symmetric vs = very strong, s = strong, m= medium, w = weak, vw = very weak

3.5 COMPUTATIONAL STUDIES

In total, six of the complexes were selected for computational analysis on the basis that they were representative of most of the important vibrations found in all the complexes. The solid state effects in the FIR region that affect the number of vibrations visible in the calculated spectra are present for these complexes as they were in Chapter 2. For this reason the FIR spectra are not shown. However, all vibrations, both observed and masked, in the calculated spectra are presented in the appropriate tables.

3.5.1 [$CrCl_3$(bipy)(thf)]

This complex was selected as it was an important indicator relevant to understanding the mechanistic pathway to complex formation, particularly with regard to the experimentally assigned thf vibrations which are indicative of the monomeric species. Figures 3.14 and 3.15 highlight the very strong correlation between the experimental and calculated spectra, from which meaningful deductions can be made. The first deduction relates to the C–H vibrations associated with the thf ligand which, with respect to these types of complex, are now confirmed as being found as definitive vibrations at lower frequencies than their aromatic heterocycle counterparts (bipyridine and pyridine). The presence of not just thf but, specifically, coordinated thf, is confirmed with the correlation of the asymmetrical ν(C–O–C) vibration found exclusively in the IR of both the experimental and calculated spectra at 1006 and 995 cm^{-1} respectively. Another characteristic thf vibration is the symmetrical ν(C–O–C) which, in direct correlation with the literature, is found at 856 cm^{-1} in this complex. Interestingly, the calculated equivalent IR and Raman spectra possess three ν(C–O–C) modes, two asymmetrical stretches at 844 and 816 cm^{-1}, in addition to one symmetrical stretch at 831 cm^{-1}. Of all the vibrations, perhaps the strongest correlation between experimental and calculated relates to the bipyridine frequencies that are found at positions inferring coordination.

Unfortunately, the specific metal–ligand vibrations in the calculated spectra cannot be easily assigned to individual vibrations as the modes are mixed.

A selection of all the important vibrations discussed above is given in Table 3.5.

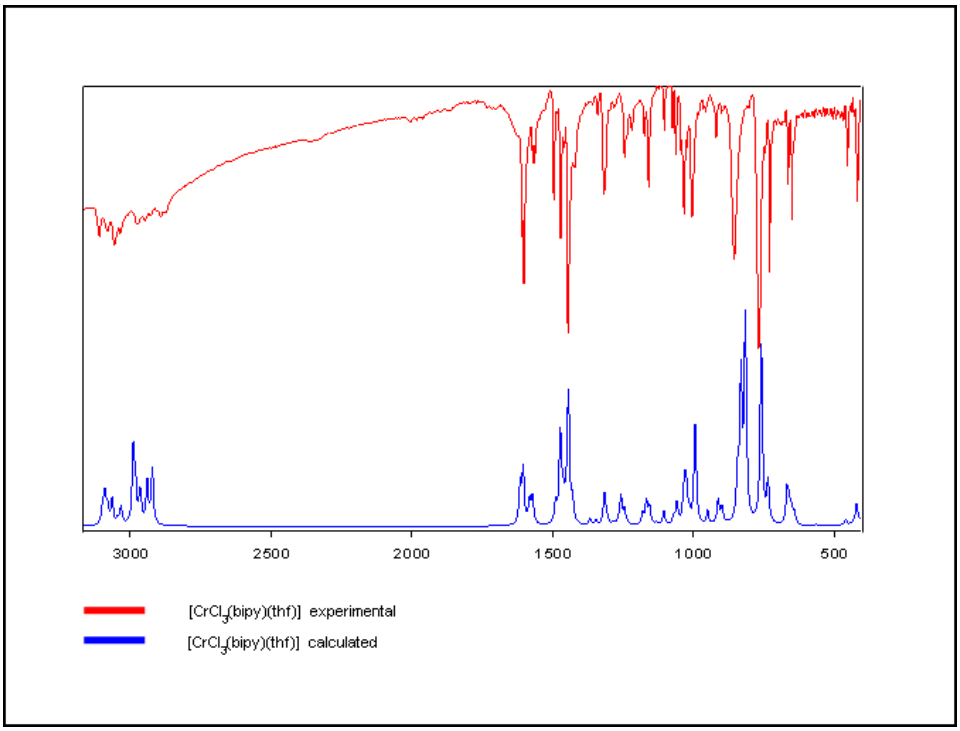

Figure 3.14 **Experimental (red) and calculated (blue) MIR spectra of $[CrCl_3(bipy)(thf)]$**

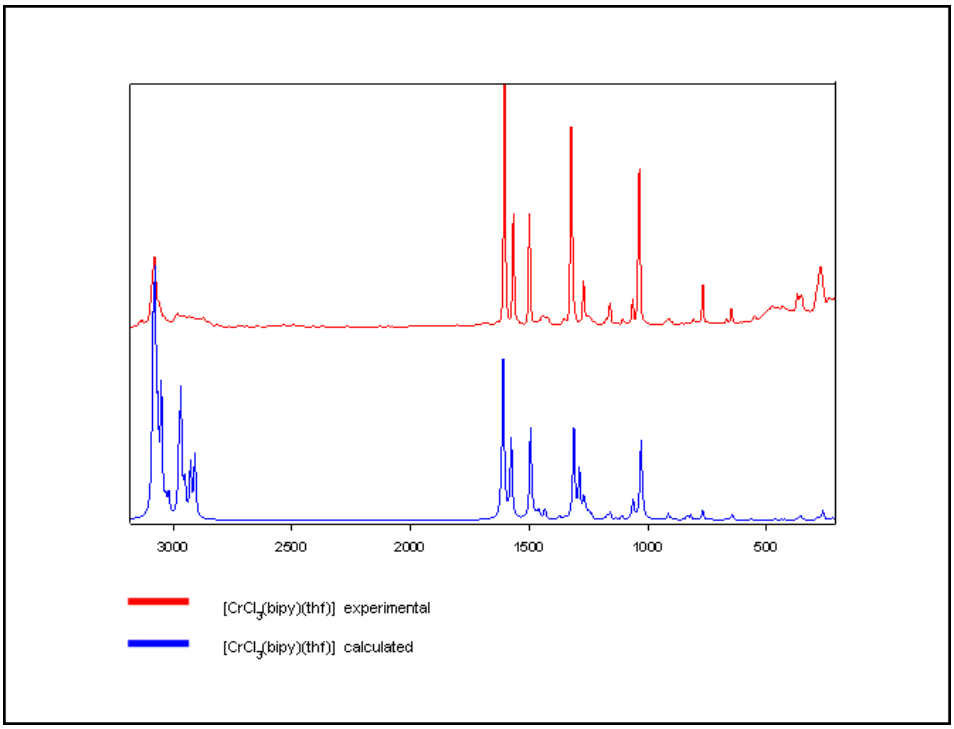

Figure 3.15 **Experimental (red) and calculated (blue) Raman spectra of $[CrCl_3(bipy)(thf)]$**

Table 3.5 **Selected experimental and calculated IR and Raman band assignments for [$CrCl_3$(bipy)(thf)]**

[$CrCl_3$(bipy)(thf)] IR / cm^{-1}		[$CrCl_3$(bipy)(thf)] Raman / cm^{-1}		Assignment	
Experimental	**Calculated**	**Experimental**	**Calculated**	**Experimental**	**Calculated**
2948	2966	2948	2968	thf ν(CH)	thf ν(CH)
2929	2941	2932	2952	thf ν(CH)	thf ν(CH)
1609, 1602	1616, 1606	1604	1606	ν_{ring} (bipy)	ν_{ring} (bipy)
1318	1317	1321	1311	ν_{ring} (CN)	ν_{ring} (CN)
1006	995	-	-	thf ν(COC) asym	thf ν(COC) asym
856	844, 831, 816	854	845, 834, 818	thf ν(COC) sym	thf ν(COC) asym, sym, asym
665	662	669	662	ν_{ring} (bipy)	ν_{ring} (bipy)
451	460	-	-	bipy ring def	bipy ring def
369, 355, 345	363, 350	369, 350, 341	364, 351	Cr-Cl	Cr-Cl + Cr-N
284	311	271	312	Cr-O	Cr-O + Cr-N
244	262	234	263	Cr-N (bipy)	Cr-Cl + thf twist

Table 3.6 **Scaling factors determined for [$CrCl_3$(bipy)(thf)]**

Region / cm^{-1}	IR	Raman
0 - 1854	0.976911	0.979130
2839 - 3422	0.961780	0.957214

3.5.2 $[CrCl_3(bipy)(H_2O)]$

The fact that this complex's crystal structure has been solved as part of this study made it an ideal choice for computational study. It is, however, unfortunate that no Raman spectrum comparisons could be made due to the sample fluorescence already discussed.

As can be seen from Figure 3.16, there is strong agreement between the experimental and calculated IR frequencies, with the one obvious exception being the O–H stretching band above 3000 cm^{-1}. Although the calculated spectrum shows two vibrations associated with the symmetrical and asymmetrical modes of O–H, it is widely accepted that a single broad band in this region is indicative of coordinated water.

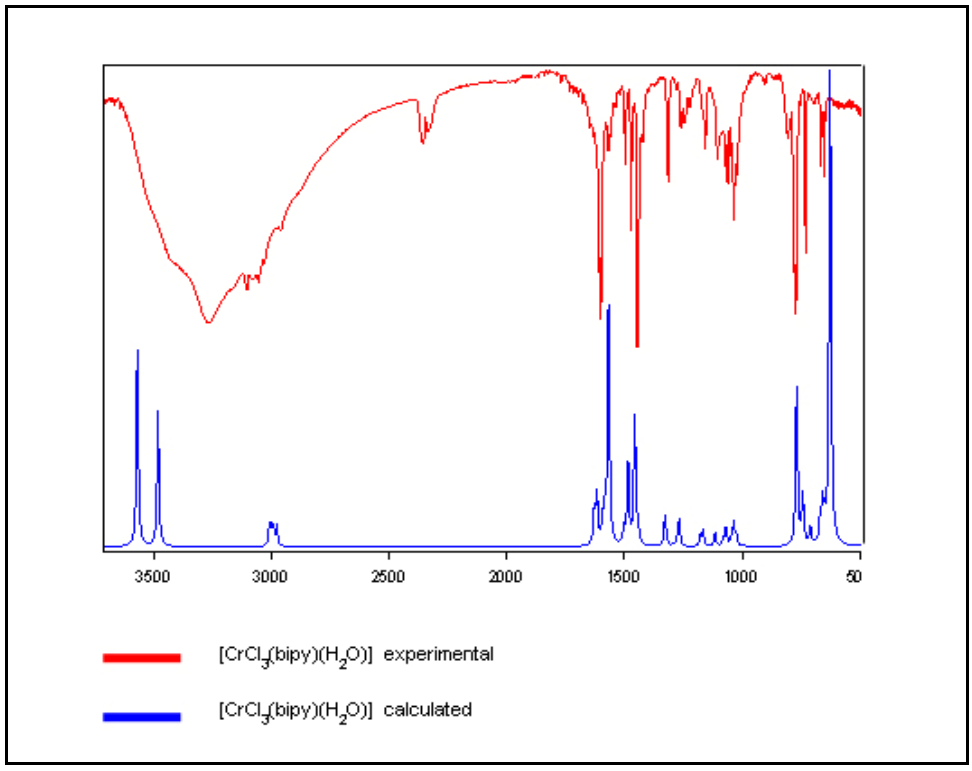

Figure 3.16 Experimental (red) and calculated (blue) MIR spectra of $[CrCl_3(bipy)(H_2O)]$

Along with a selection of other characteristic vibrations, Table 3.7 shows that the presence of coordinated water is confirmed, with the calculated data agreeing with the experimental assignment found just above 1600 cm^{-1}. The assignments of bipyridine-specific vibrations is also confirmed, which therefore indicates coordination.

Of the metal–ligand vibrations, the Cr–Cl modes show the strongest correlation, although, as with the Cr–O and Cr–N modes, the expected third vibration in the calculated spectrum was mixed with other vibrations.

Table 3.7 **Selected experimental and calculated IR band assignments for [$CrCl_3(bipy)(H_2O)$]**

[$CrCl_3(bipy)(H_2O)$] IR / cm^{-1}		**Assignment**	
Experimental	**Calculated**	**Experimental**	**Calculated**
3278	3574, 3490	ν(OH)	ν (OH) sym, asym
1608	1620	H-O-H	H-O-H + ν_{ring}
1570	1567	ν_{ring}	O-H scissors
1313	1332	ν_{ring} (CN)	ν_{ring} (CN)
451	462	bipy ring def	bipy ring def
416	424	bipy ring def	bipy ring def
-	390	-	Cr-O
371, 355, 346	360, 354	Cr-Cl	Cr-Cl
284	279	ν_{ring} / Cr-O	Cr-N + Cr-O + Cr-Cl
242	259, 232	Cr-N	Cr-N + Cr-O + Cr-Cl

Table 3.8 **Scaling factors determined for [$CrCl_3(bipy)(H_2O)$]**

Region / cm^{-1}	**Infrared**
0 – 1861	0.984833
2988 – 3422	0.935161

3.5.3 [$CrCl_3$(bipy)(CH_3CN)]

This complex was selected for computational investigation because it is the only one in this class to offer a non–pyridine-based monodentate N–type ligand and because the ligand itself possesses a number of characteristic vibrations.

The findings presented in Figures 3.17 and 3.18 show strong agreement between the experimental and computational values of the IR and Raman spectra.

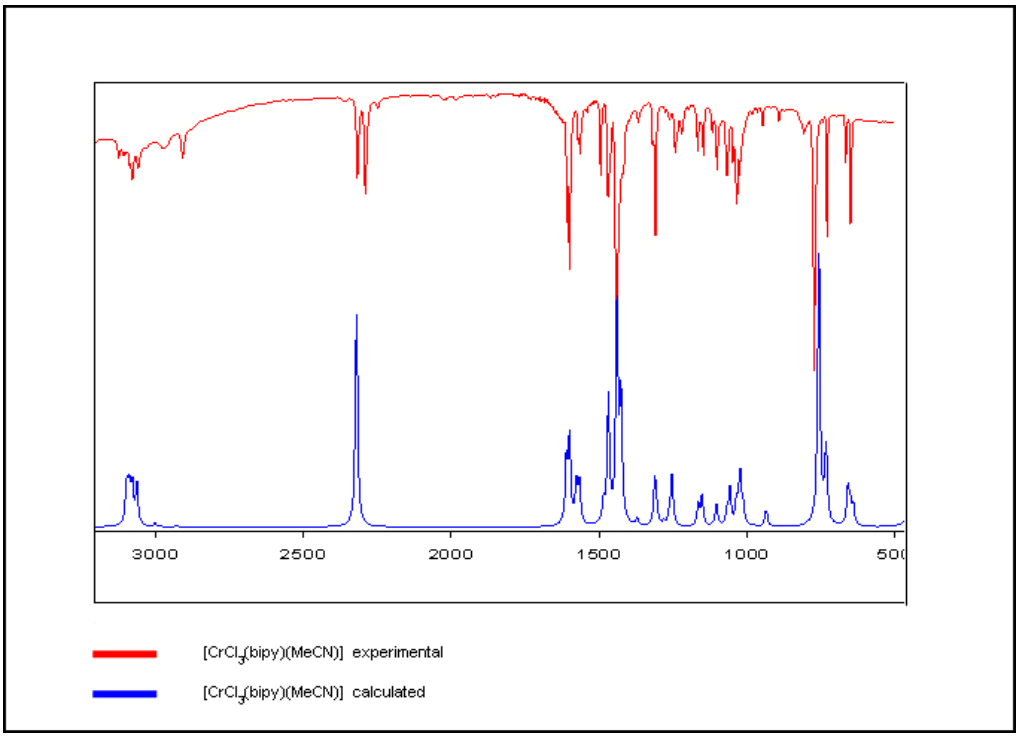

Figure 3.17 Experimental (red) and calculated (blue) MIR spectra of [$CrCl_3$(bipy)(CH_3CN)]

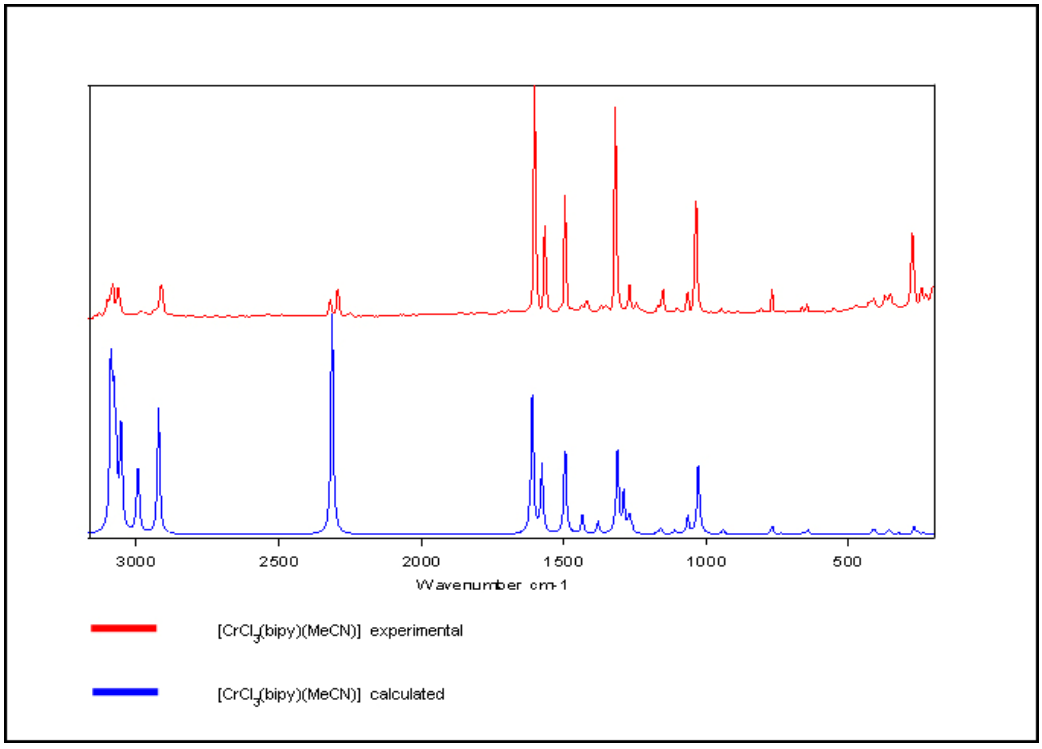

Figure 3.18 Experimental (red) and calculated (blue) Raman spectra of [$CrCl_3$(bipy)(CH_3CN)]

The only obvious difference is in the number of CH_3CN vibrations found between 2000 and 2500 cm^{-1}. Although it has already been mentioned in the vibrational discussions above, it is worth reiterating that all the previous literature on CH_3CN vibrations concurs with the two bands observed in the experimental spectra. These, along with a selection of other important ligand vibrations found in the complex, are highlighted in Table 3.9.

As in the previous complexes, the metal–ligand vibrational comparisons are again hampered by the mixing of modes in the calculated spectra to the extent that a clear distinction is not even made between the very different Cr–N (bipy) and Cr–N (CH_3CN) environments. This does to some extent, however, add weight to the conclusions drawn in the literature-based experimental assignments whereby no Cr–N (CH_3CN)-specific vibration was defined.

Table 3.9 **Selected experimental and calculated IR and Raman band assignments for [$CrCl_3$(bipy)(CH_3CN)]**

[$CrCl_3$(bipy)(CH_3CN)] IR /cm^{-1}		$CrCl_3$(bipy)(CH_3CN)] Raman/cm^{-1}		Assignment	
Experimental	**Calculated**	**Experimental**	**Calculated**	**Experimental**	**Calculated**
2910	2933	2913	2922	ν (CH_3) sym	ν (CH_3) sym
2318	-	2321	-	δ(CH_3) sym + ν(CC) (MeCN)	-
2291	2321	2293	2312	ν (C≡N)	ν (C≡N)
1608, 1600	1610, 1602	1600	1609	ν_{ring}	ν_{ring}
1367	1370	1367	1379	(CH_3) asym def	CH_3 def
1318, 1309	1311	1317	1315	ν_{ring} (CN)	ν_{ring} (CN)
664	658	665	653	ν_{ring} (bipy)	ν_{ring} (bipy)
454	459	-	-	bipy ring def	bipy ring def
365, 352, 337	357, 349	369, 350, 336	360, 350	Cr-Cl	Cr-Cl + Cr-N (bipy) + MeCN wag
-	322	-	322	-	Cr-N (bipy) + Cr-N (MeCN)
243	236	244	237	Cr-N (bipy)	Cr-Cl + Cr-N (MeCN) + bipy rock

ν = stretching, δ = in plane bending, def = deformation

Table 3.10 **Scaling factors determined for [$CrCl_3$(bipy)(CH_3CN)]**

Region / cm^{-1}	IR	Raman
0 – 1854	0.973658	0.979560
2213 – 3423	0.962099	0.958557

3.5.4 [$CrCl_3$(bipy)(py)]

Of particular interest with this compound was whether the assignments made to the experimental spectrum with regard to differentiating between bipyridine and pyridine vibrations could be supported. What aided this investigation was the extremely good match between the experimental and calculated vibrations seen in Figures 3.19 and 3.20.

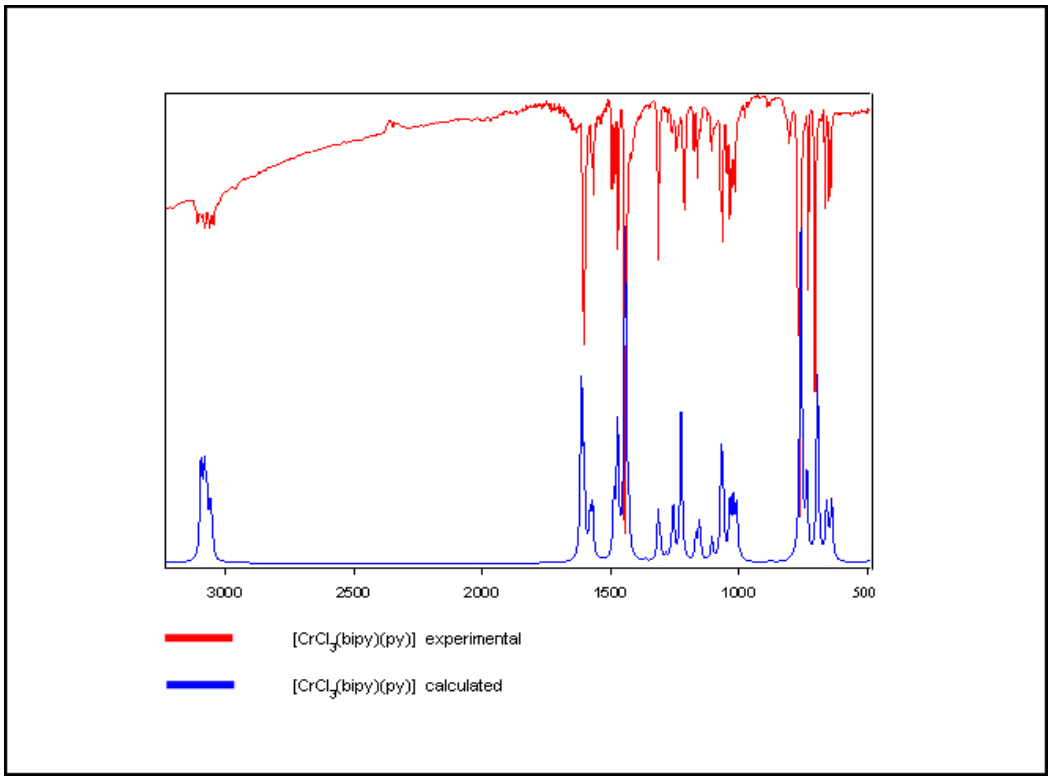

Figure 3.19 **Experimental (red) and calculated (blue) MIR spectra of [$CrCl_3$(bipy)(py)]**

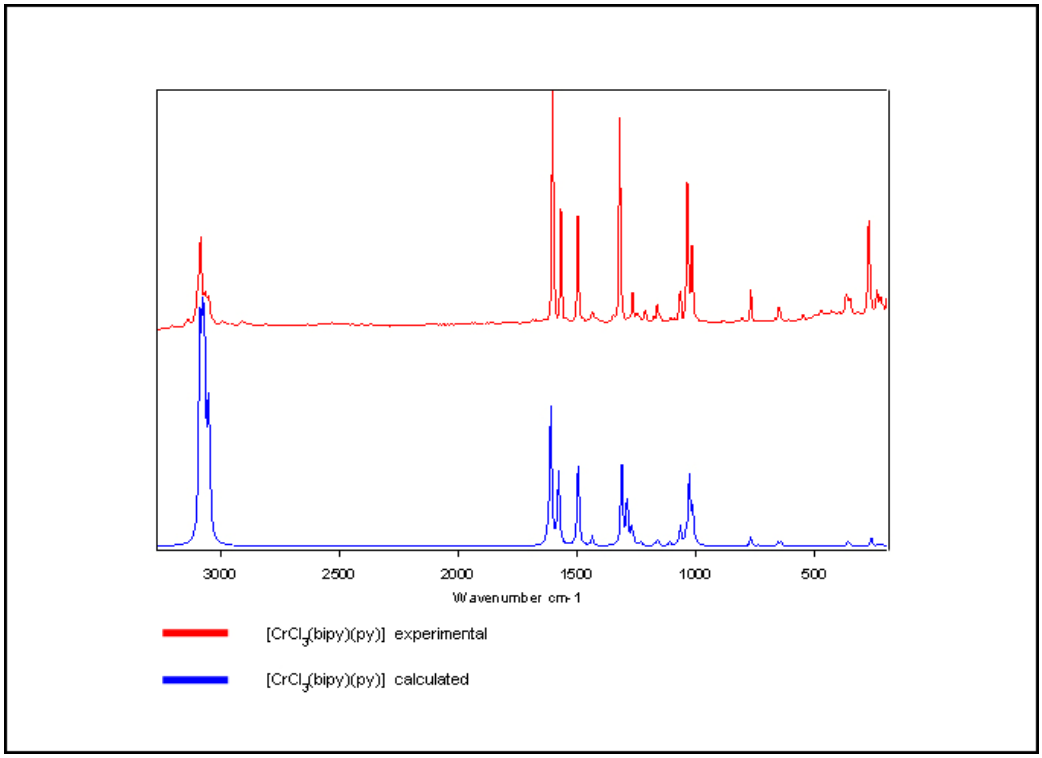

Figure 3.20 Experimental (red) and calculated (blue) Raman spectra of [$CrCl_3$(bipy)(py)]

As can been seen in Table 3.11, which highlights the important vibrations, computationally backed differences between the two heterocyclic N–ligands can be confirmed; these are all found at positions indicative of coordination.

Unfortunately, the same cannot be said for the Cr–N vibrations as, rather surprisingly, the calculated data makes no distinction between the two ligand environments and finds them both to be at ~305 cm^{-1}. As with [$CrCl_3$(bipy)(py)], the mixing of vibrations allows only two clear Cr–Cl vibrations to be observed in the calculated spectrum.

Table 3.11 **Selected experimental and calculated IR and Raman band assignments for [$CrCl_3$(bipy)(py)]**

[$CrCl_3$(bipy)(py)] IR / cm^{-1}		$CrCl_3$(bipy)(py)] Raman / cm^{-1}		Assignment	
Experimental	**Calculated**	**Experimental**	**Calculated**	**Experimental**	**Calculated**
1607	1613	-	-	ν_{ring} (py)	ν_{ring} (bipy + py)
1602	1604	1604	1610	ν_{ring} (bipy)	ν_{ring} (bipy)
1566	1570	1567	1577	ν_{ring} (bipy)	ν_{ring} (bipy)
1313	1315	1321	1312	ν_{ring} (CN)	ν_{ring} (CN)
1013	1008	1016	1012	Ring breathing (py)	Ring breathing (py)
663	657	663	652	ν_{ring} (bipy)	ν_{ring} (bipy)
643	636	-	-	δ_{ring} (py)	δ_{ring} (py)
453	459	470	462	bipy ring def	bipy ring def
442	443	442	445	ν_{ring} (py)	ν_{ring} (py) + weak ν_{ring} (bipy)
360, 348, 319	359, 345	365, 350, 317	360, 345	Cr-Cl	Cr-Cl
-	305	-	306	-	Cr-N (bipy + py)
236	231	236	231	Cr-N (bipy)	Cr-Cl + bipy rock + py rock
222	217	222	217	Cr-N (py)	Cr-Cl + bipy rock + py rock

ν = stretching, δ = in-plane bending, def = deformation

Table 3.12 Scaling factors determined for [$CrCl_3$(bipy)(py)]

Region / cm^{-1}	IR	Raman
0 - 1854	0.975740	0.980158
2980 - 3425	0.960663	0.957941

3.5.5 [$CrCl_3$(bipy)(pyphenyl)]

Computational analysis was conducted on this complex as the experimental analysis (literature) indicated that there may be coordinated thf present and that the complex may in fact be a mixture. With the strong correlation between the experimental and calculated spectra shown in Figures 3.21 and 3.22, positive deductions could be made.

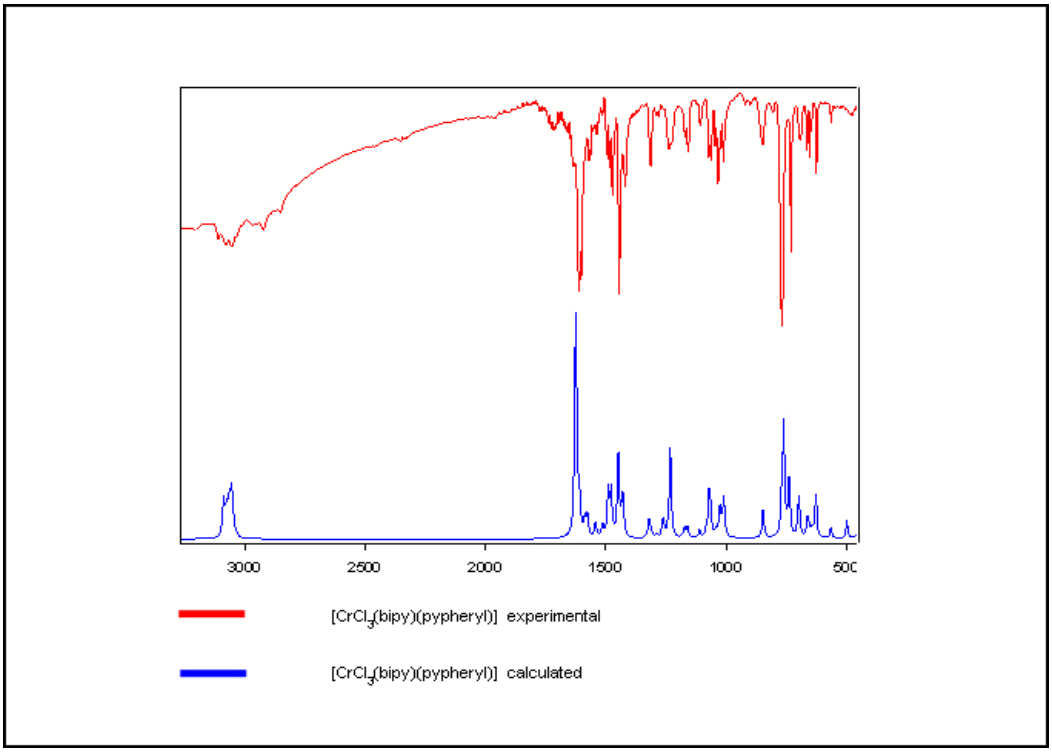

Figure 3.21 Experimental (red) and calculated (blue) MIR spectra of [$CrCl_3$(bipy)(pyphenyl)]

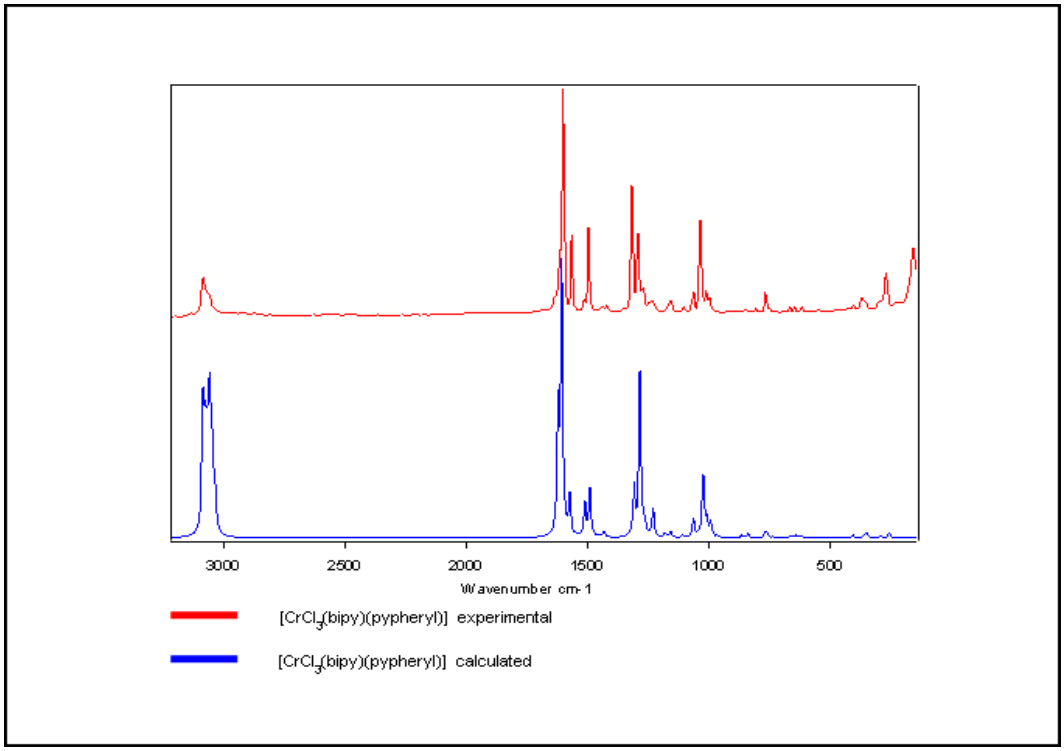

Figure 3.22 Experimental (red) and calculated (blue) Raman spectra of [$CrCl_3$(bipy)(pyphenyl)]

The reason that a mixture is suspected is due to the presence of the band at 856 cm^{-1} associated with coordinated thf (C–O–C). However, as a result of the computational data this band can now be assigned with confidence to a pyphenyl-specific vibration. If one then assumes that the C–H vibrations previously assigned to thf (2948, 2892 cm^{-1}) are associated with free thf (since a distinction between free and coordinated is most difficult), then there is sufficient evidence to suggest that this is not a mixture.

A summary of the important vibrations is given in Table 3.13 in which, in addition to the above-mentioned 856 cm^{-1} mode, one is able to see the strong agreement between the experimental and calculated assignments of both the bipyridine and pyphenyl vibrations.

With regard to the metal–ligand vibrations, the same trend is followed as with the other bipyridine complexes whereby only two distinct Cr–Cl vibrations are observed in the calculated spectra, with more observed as mixed vibrations at lower frequencies. However, unlike [$CrCl_3$(bipy)(py)], an obvious Cr–N vibration associated with the pyphenyl coordination is observed in the calculated IR spectrum at

348 cm^{-1}. Unfortunately, the same cannot be said regarding the Cr–N bipy equivalent, which is seen as a mixed mode at 293 cm^{-1}.

Table 3.13 **Selected experimental and calculated IR and Raman band assignments for [$CrCl_3$(bipy)(pyphenyl)]**

[$CrCl_3$(bipy)(pyphenyl)] IR / cm^{-1}		$CrCl_3$(bipy)(pyphenyl)] Raman / cm^{-1}		Assignment	
Experimental	**Calculated**	**Experimental**	**Calculated**	**Experimental**	**Calculated**
1610	1625	1613	1622	ν_{ring} (pyphenyl)	ν_{ring} (pyphenyl)
1602	-	1600	1606	ν_{ring} (bipy)	ν_{ring} (bipy)
1513	1513	1513	1511	ν_{ring} (pyphenyl)	ν_{ring} (pyphenyl)
1313	1320	1317	1309	ν_{ring} (CN)	ν_{ring} (CN)
1291	1292	1292	1285	ν_{ring} (bipy) + ν_{ring} pyphenyl	ν_{ring} (bipy) + ν_{ring} pyphenyl
1011	1010	1011	1008	Ring breathing (pyphenyl)	Ring breathing (pyphenyl)
856	856	849	863	Coord thf	δ_{ring} (pyphenyl)
625	627	616	620	δ_{ring} (pyphenyl)	δ_{ring} (pyphenyl)
454	462	-	-	bipy ring def	bipy ring def
419	419	424	434	bipy ring def	bipy ring def
-	389	-	-	-	δ_{ring} (pyphenyl)

372, 355, 323	364, 340	369, 352, 304	363, 340	Cr-Cl	Cr-Cl
-	348	-	-	-	Cr-N (pyphenyl)
-	293	-	292	-	Cr-N (bipy + pyphenyl)
236	229	232	229	Cr-N (bipy)	Cr-Cl + bipy rock + py rock
209	217	213	216	Cr-N (pyphenyl)	Cr-Cl + bipy rock + py rock

ν = stretching, δ = in-plane bending, def = deformation

Table 3.14 Scaling factors determined for [$CrCl_3$(bipy)(pyphenyl)]

Region / cm^{-1}	IR	Raman
0 – 1859	0.979713	0.977676
2966 – 3424	0.958930	0.957493

3.5.6 [$HpyNH_2$][$CrCl_4$(bipy)]

In contrast to the similar cationic-anionic crystal structure [Hpy][$CrCl_4(py)_2$] that was determined in Chapter 2, it was possible to collect IR and Raman data for this compound. This therefore allowed theoretical spectra to be generated and comparisons carried out with the corresponding experimental spectra. The fact that the calculations ignored the DCM molecule encaptured as part of the crystal structure was of little importance as no evidence of this molecule was found in the experimental IR or Raman spectra due to evaporation.

While Figures 3.23 and 3.24 indicate the good correlations between the respective theoretical and experimental spectra, it is the assignment comparisons of key bands presented in Table 3.15 that emphasise the true strength of these correlations.

Unfortunately, the mixing of modes in the calculated spectra inhibited the assignment of specific metal–ligand vibrations.

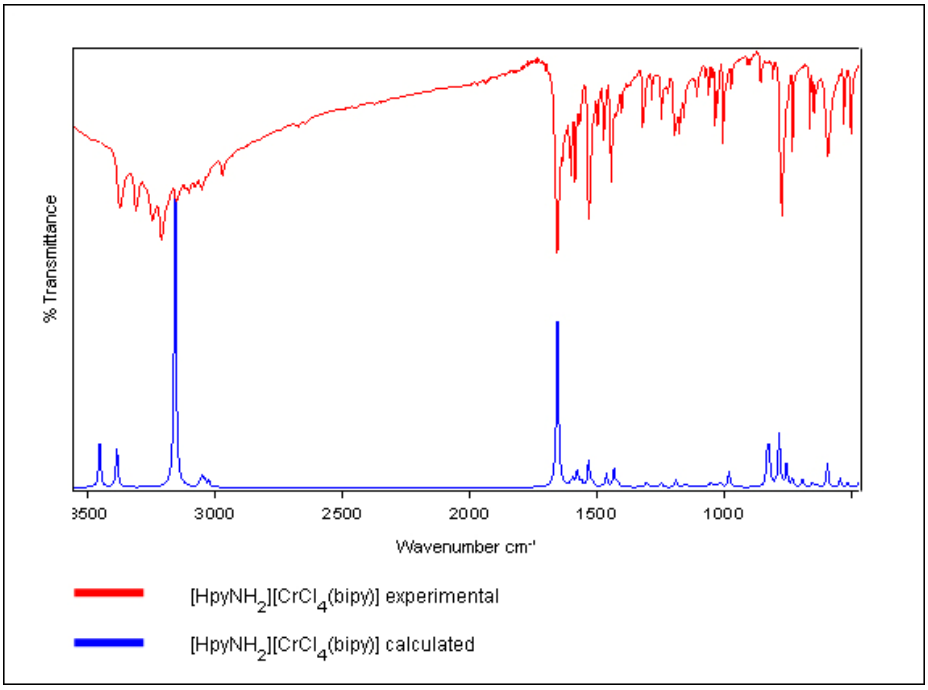

Figure 3.23 Experimental (red) and calculated (blue) Raman spectra of $[HpyNH_2][CrCl_4(bipy)]$

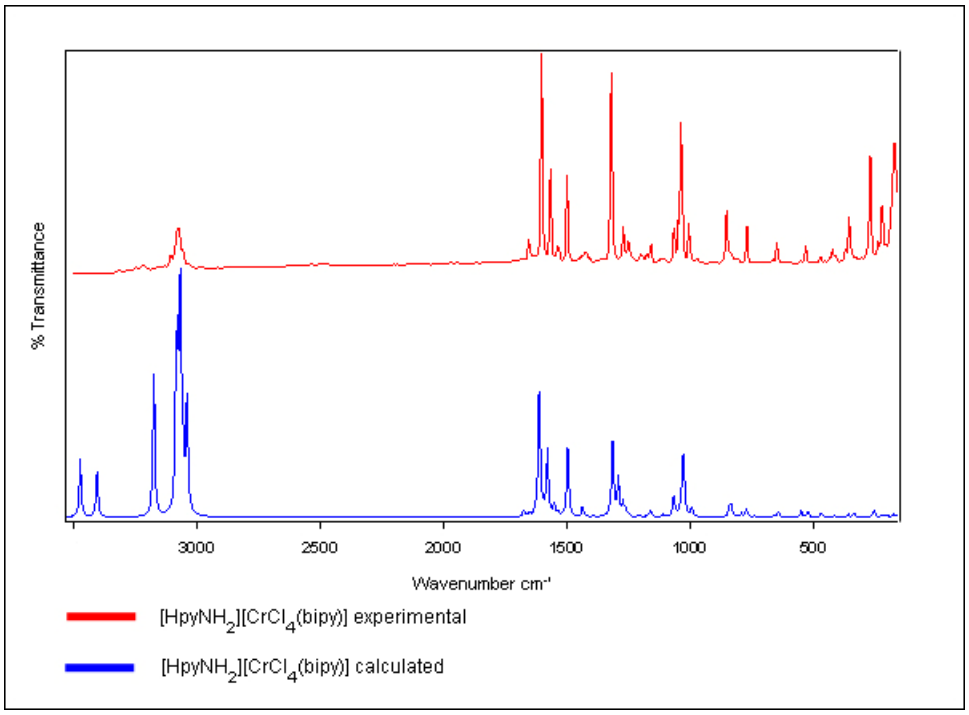

Figure 3.24 Experimental (red) and calculated (blue) Raman spectra of $[HpyNH_2][CrCl_4(bipy)]$

Table 3.15 **Selected experimental and calculated IR and Raman band assignments for $[HpyNH_2][CrCl_4(bipy)]$**

$[HpyNH_2][CrCl_4(bipy)]$ IR / cm^{-1}		$[HpyNH_2][CrCl_4(bipy)]$ Raman / cm^{-1}		Assignment	
Experimental	**Calculated**	**Experimental**	**Calculated**	**Experimental**	**Calculated**
3153	3157	3142	3173	$\nu(NH_2)$ sym	$\nu(NH_2)$ asym
1656	1655	1653	1654	$\delta(NH_2)$	$\delta(NH_2) + \nu_{ring}$
1600	1592	1601	1610	ν_{ring} (bipy)	ν_{ring} (bipy)
1585	1576	-	-	pyH (CC)	pyH (CC)
1318	1305	1318	1320	ν_{ring} (CN)	ν_{ring} (CN)
661	652	661	653	ν_{ring} (bipy)	ν_{ring} (bipy)
642	631	646	639	pyH (CCC)	pyH (CCC)
590	592	597	598	pyH (CC)	pyH (N^+H)
452	456	452	461	bipy ring def	bipy ring def
366, 350, 343, 327	330	367, 352, 326	334	Cr-Cl	Cr-Cl
-	327, 311	-	331, 314	-	Cr-Cl + Cr-N
-	248, 220	-	250, 223	-	Cr-Cl + bipy rock
237	-	235	-	Cr-N	-
220	211	220	213	pyH	pyH

ν = stretching, δ = in-plane bending, def = deformation

Table 3.16 **Scaling factors determined for $[HpyNH_2][CrCl_4(bipy)]$**

Region / cm^{-1}	IR	Raman
0 – 1854	0.969057	0.980070
2980 – 3425	0.950532	0.954942

3.5.7 HOMO AND LUMO ORBITALS OF THE CALCULATED COMPLEXES

In the case of all the complexes discussed in Chapter 2 the chlorine atoms are sites of high electron density and are susceptible to electrophilic attack. However, what is perhaps surprising is that the various monodentate ligands that differ both sterically and electronically from each other do not play a role in altering the region of nucleophilic attack, which in all cases is found to be the bipyridine ligand. The same trend holds true for $[HpyNH_2][CrCl_4(bipy)]$. Figures 3.25-3.30 depict the HOMO and LUMO orbitals of the compounds.

HOMO **LUMO**

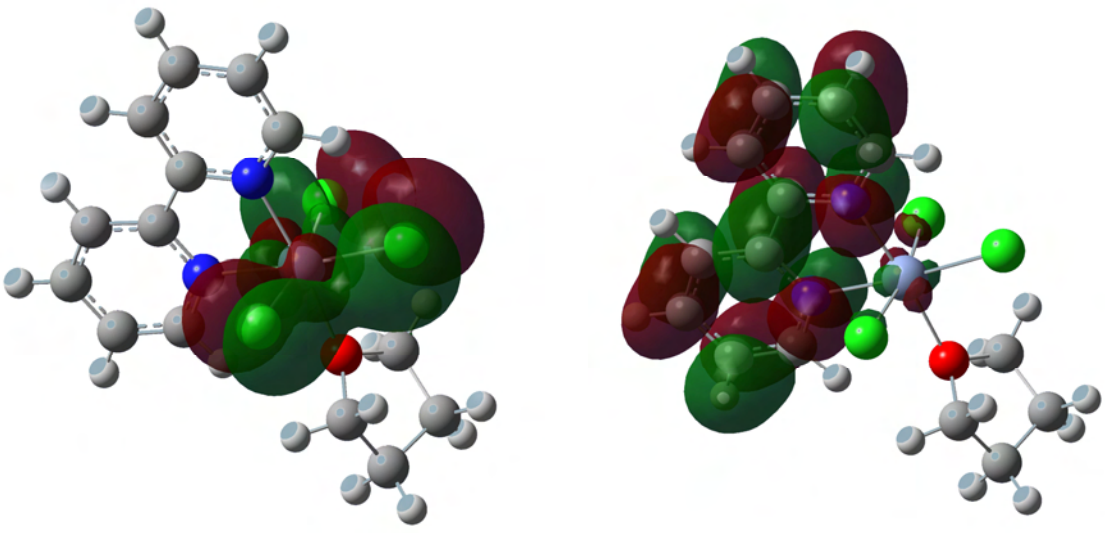

Figure 3.25 **HOMO and LUMO orbitals of $[CrCl_3(bipy)(thf)]$**

HOMO **LUMO**

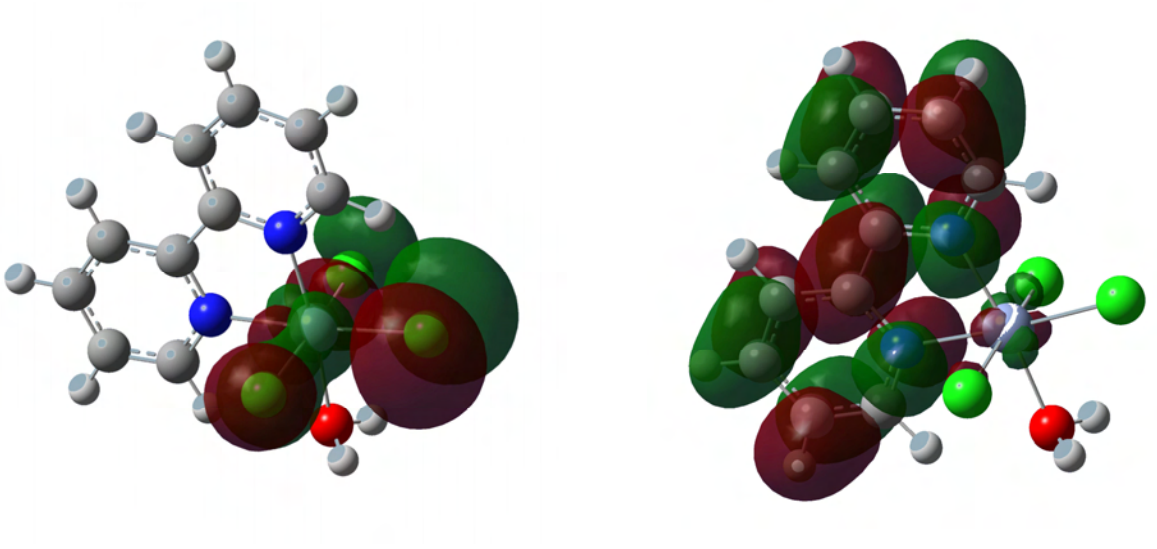

Figure 3.26 **HOMO and LUMO orbitals of [$CrCl_3$(bipy)(H_2O)]**

HOMO **LUMO**

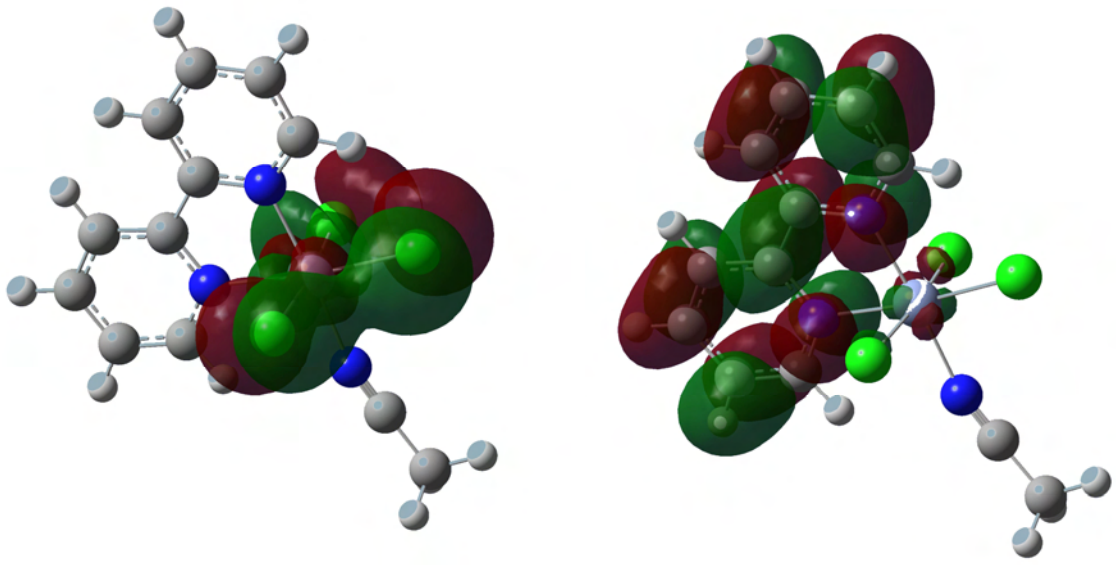

Figure 3.27 **HOMO and LUMO orbitals of [$CrCl_3$(bipy)(MeCN)]**

HOMO **LUMO**

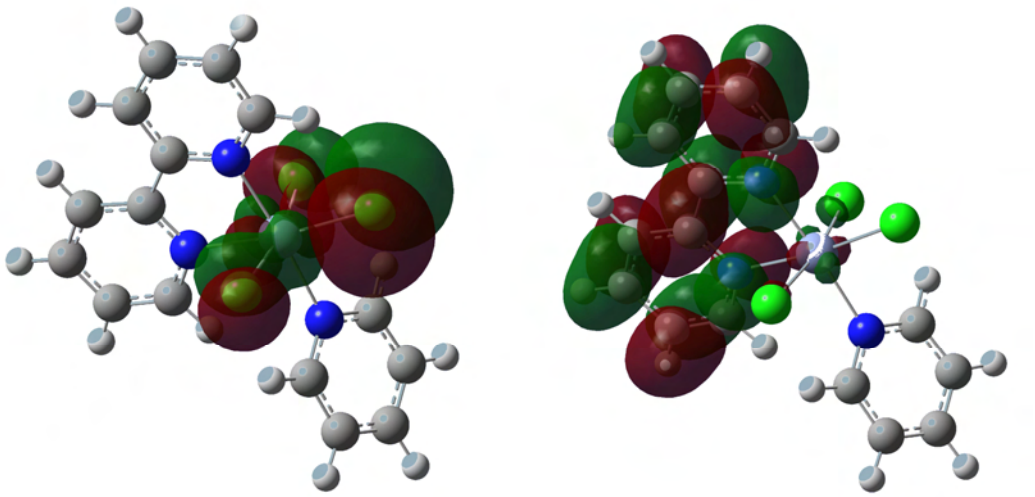

Figure 3.28 **HOMO and LUMO orbitals of [$CrCl_3$(bipy)(py)]**

HOMO **LUMO**

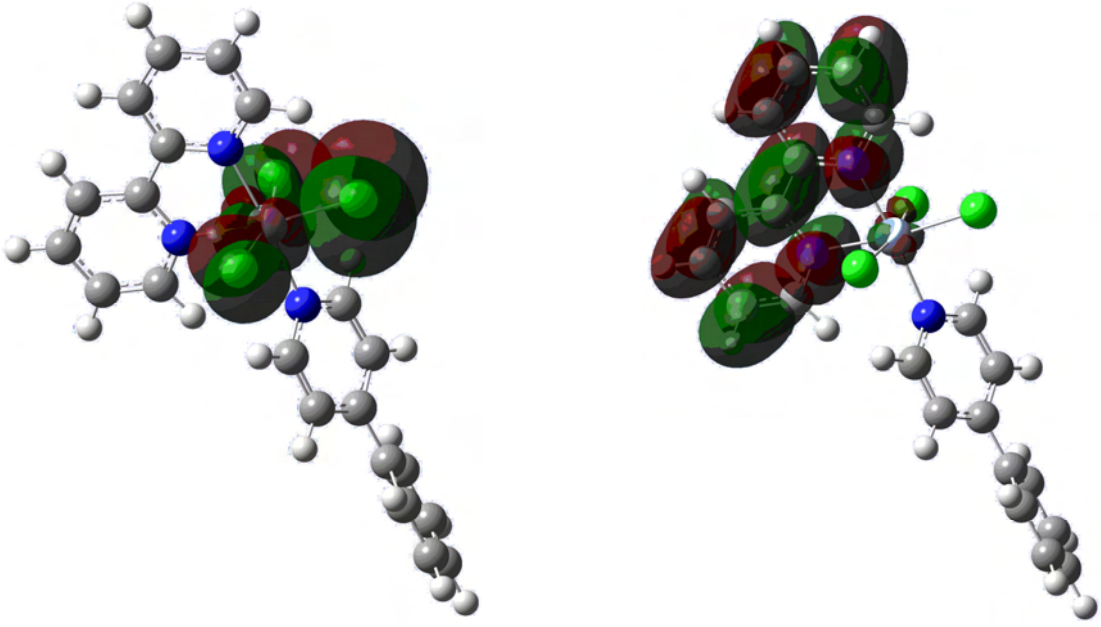

Figure 3.29 **HOMO and LUMO orbitals of [$CrCl_3$(bipy)(pyphenyl)]**

HOMO **LUMO**

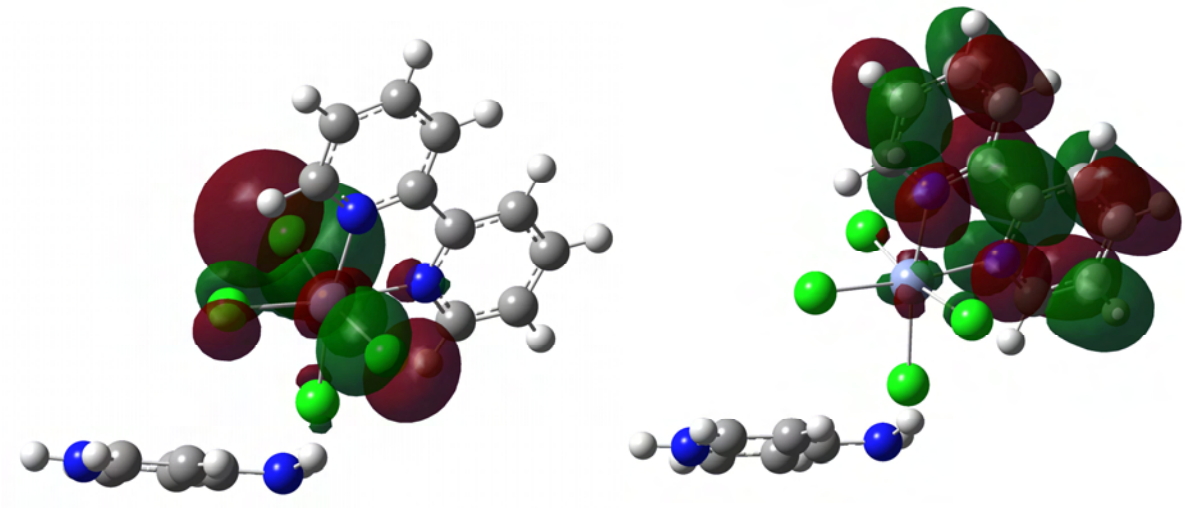

Figure 3.30 HOMO and LUMO orbitals of [HpyNH$_2$][CrCl$_4$(bipy)]

3.6 NMR SPECTROSCOPY

In the light of the success achieved in being able to follow the substitution of thf with monodentate pyridine ligands via ^{1}H NMR spectroscopy (as seen in Chapter 2), an analogous experiment was carried out whereby one equivalent of bipyridine was added to the [CrCl$_3$(thf)$_3$] precursor. The results were equally satisfactory.

The same procedure was employed, which involved the addition of stoichiometric amounts of bipyridine in acetone-d$_6$ to [CrCl$_3$(thf)$_3$] in an NMR tube. As expected, the result of collecting spectra in rapid succession was that the resonances associated with the free aromatic N–donor ligand (δ=7.49–8.62 ppm) disappeared upon coordination to the paramagnetic metal centre over time. See Figure 3.31.

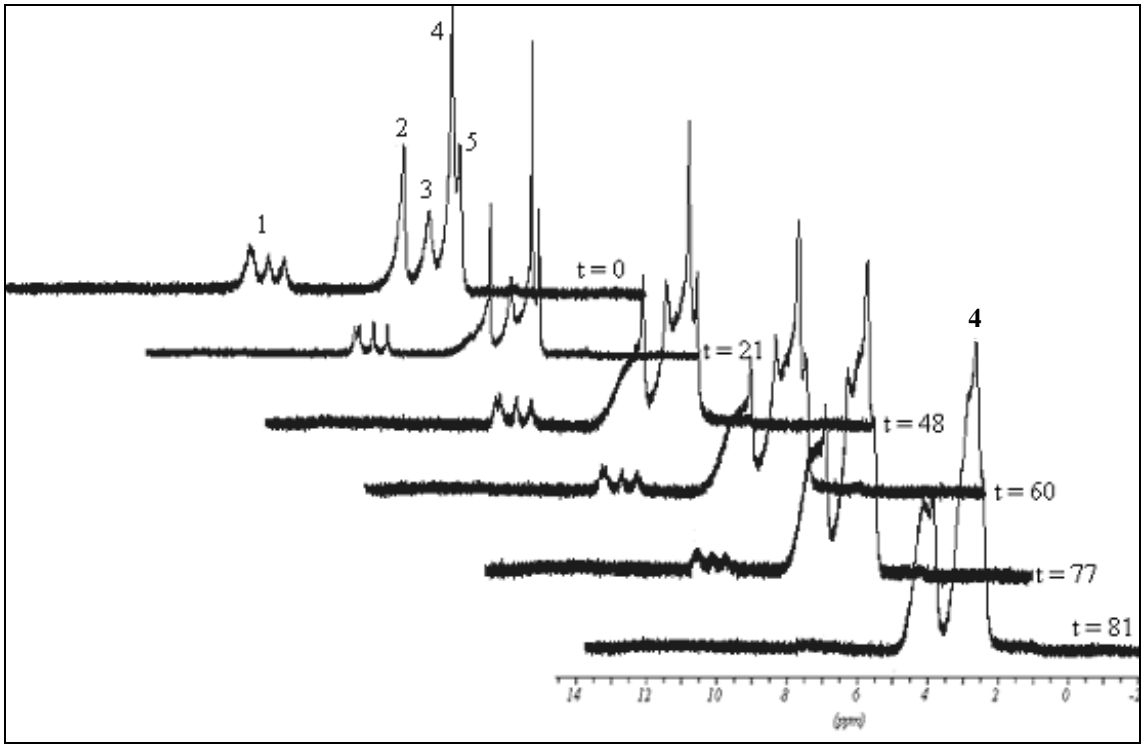

Figure 3.31 **Stacked ^{1}H NMR spectra for the reaction of bipy with $[CrCl_3(thf)_3]$ over time. 1 = bipy, 2 = thf, 3 = water peak in acetone, 4 = acetone d_6 , 5 = thf**

An integration of the resonances of uncoordinated bipyridine to the thf resonances was plotted as a ratio vs time in Figure 3.32. It can be clearly seen that the value of the ratio bipyridine:thf decreases linearly over time.

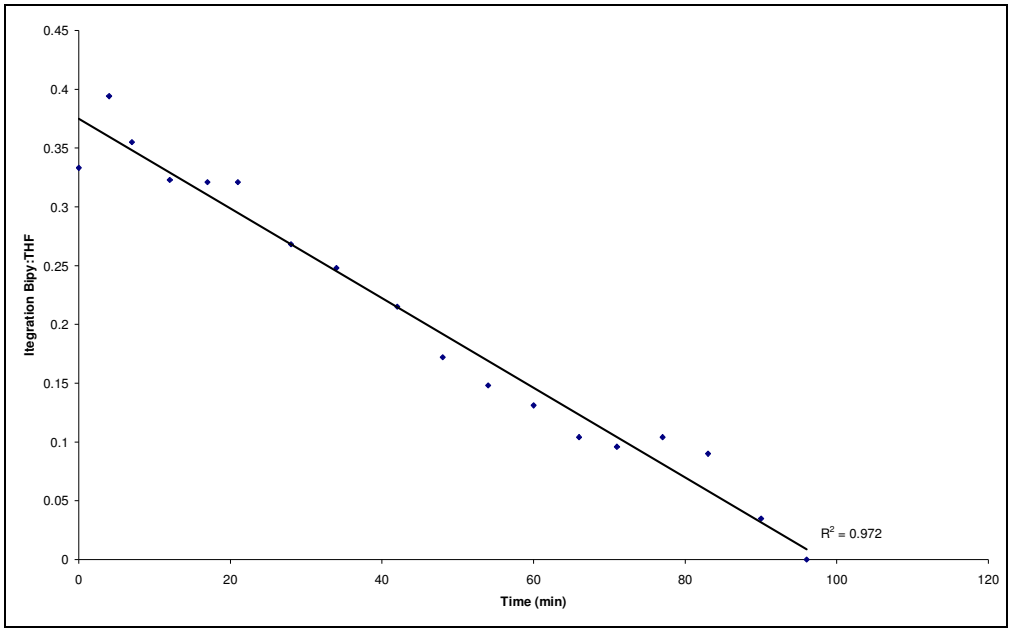

Figure 3.32 **Plot of integration of bipy:thf resonances over time**

In contrast to the pyridine results, the reaction was complete after 81 minutes and, unlike the monodentate results, this completion time coincided well with the visual observations of product formation made with the naked eye while the same reaction was being carried out under standard Schlenk conditions in the laboratory.

In keeping with the methodology of Chapter 2, the sample was left in the instrument for a further hour, after which time another spectrum was recorded (see Figure 3.33). As was the case with the analogous pyridine experiment, the spectral resonances were more defined.

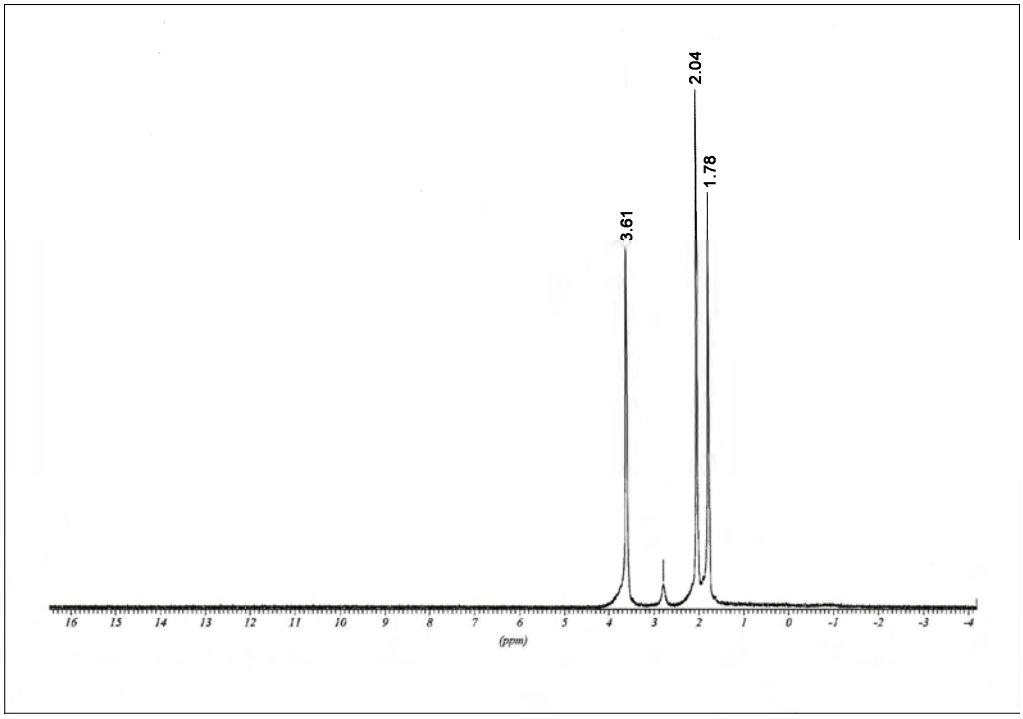

Figure 3.33 **^{1}H NMR spectra of [$CrCl_3$(bipy)(thf)] final product in acetone-d_6**

Again, the pyridine experiments were followed; a small amount of the expected olive green precipitate was dried and dissolved in DMSO-d_6 and a ^{13}C NMR spectrum recorded, Figure 3.34. The absence of bipyridine resonances suggests coordination as was the case for the monomer (pyridine) while, unlike in the previous chapter, the presence of thf resonances is indicative of coordinated thf which would be in agreement with the IR and Raman results indicating the formation of the monomer [$CrCl_3$(bipy)(thf)].

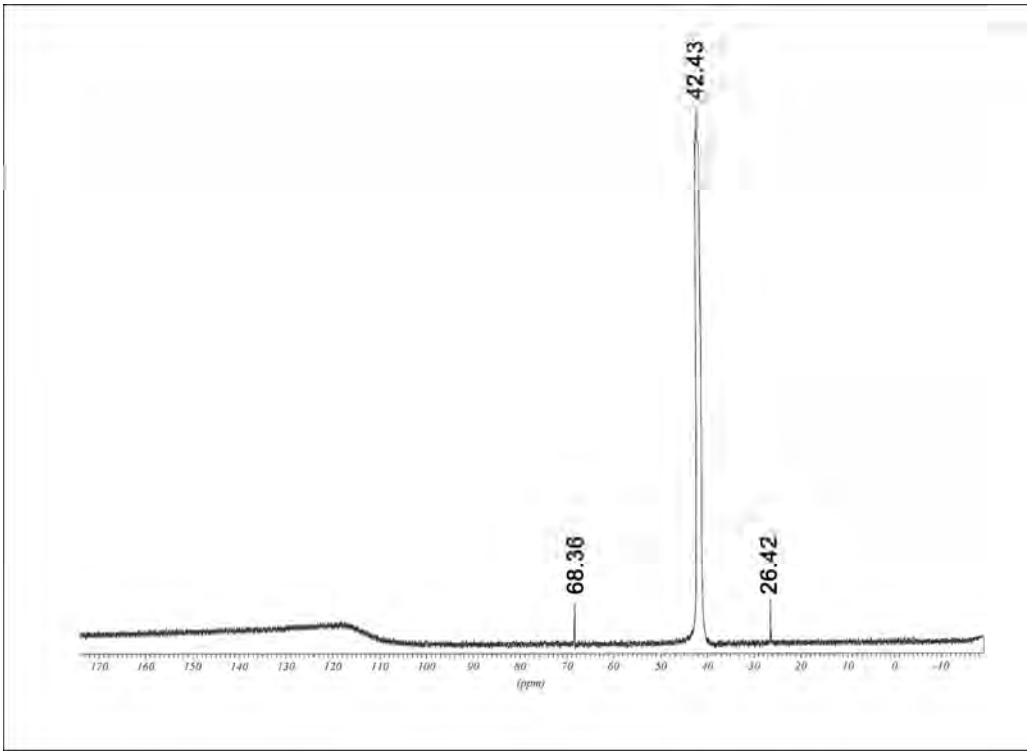

Figure 3.34 **^{13}C NMR spectrum of [$CrCl_3$(bipy)(thf)] final product in DMSO-d_6**

In an attempt to confirm that the thf resonances in the above compound were associated with the coordinated ligand, ^{1}H NMR spectra of a selection of some of the other compounds synthesised in this particular bipyridine class were studied. They included [$CrCl_3$(bipy)(CH_3CN)], [$CrCl_3$(bipy)(H_2O)] and [$CrCl_3$(bipy)(py)]. Figures 3.35 ([$CrCl_3$(bipy)(CH_3CN)]) and 3.36 ([$CrCl_3$(bipy)(py)]) are the analogous spectra to that of [$CrCl_3$(bipy)(thf)] in Figure 3.33. Figure 3.37 was recorded using DMSO-d_6 as it was the final precipitate.

Nevertheless, in all three cases bipyridine and thf resonances are absent, with the latter possibly implying coordination of the monodentate ligands. Yet further evidence of monodentate ligand coordination is observed in [$CrCl_3$(bipy)(CH_3CN)] and [$CrCl_3$(bipy)(py)] in that these monodentate ligand resonances are also absent in the respective product spectra (7.30–8.57 ppm and 1.9 ppm respectively). As the water molecule is observed at 3.3 ppm there is a suggestion that coordination to the metal has not taken place. This inability to suggest H_2O coordination via ^{1}H NMR is of no real concern as the crystal structure has been solved as part of this study.

Comparisons of these three compounds' spectra with that of $[CrCl_3(thf)_3]$ and bipyridine therefore suggest that the thf observed in the final spectrum is indicative of coordinated thf and thus the formation of $[CrCl_3(bipy)(thf)]$.

Note that the NMR deductions regarding all these compounds correlate well with the IR and Raman spectra deductions regarding the respective final products.

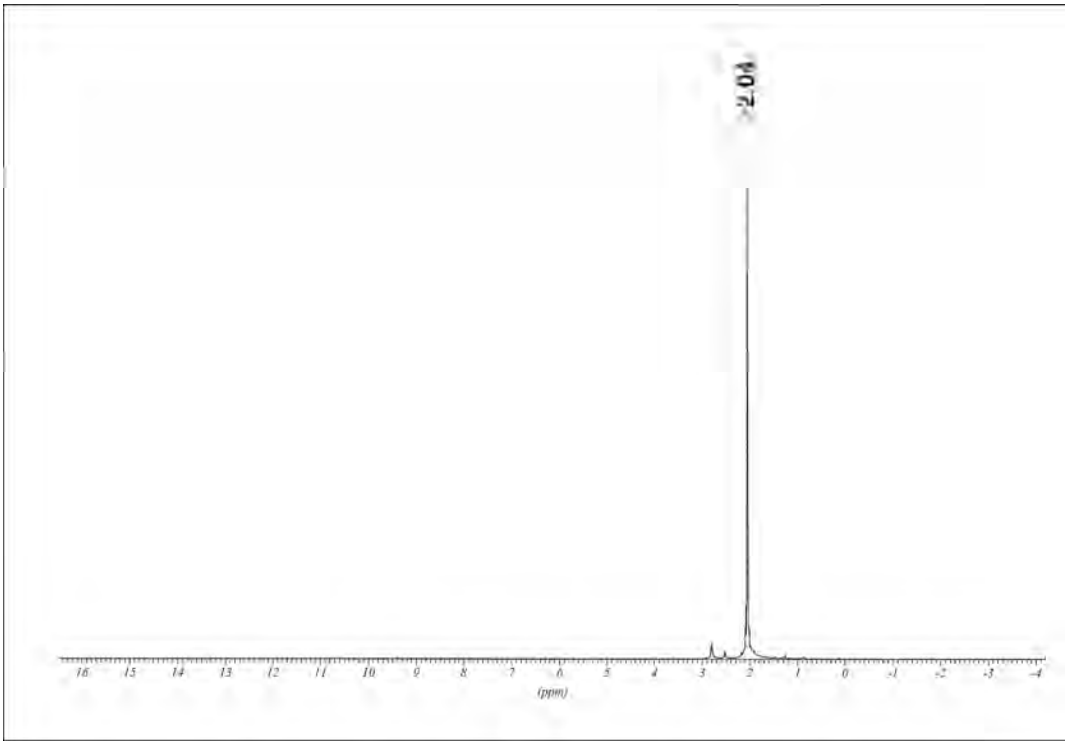

Figure 3.35 **^{1}H NMR spectrum of $[CrCl_3(bipy)(CH_3CN)]$ in acetone-d_6**

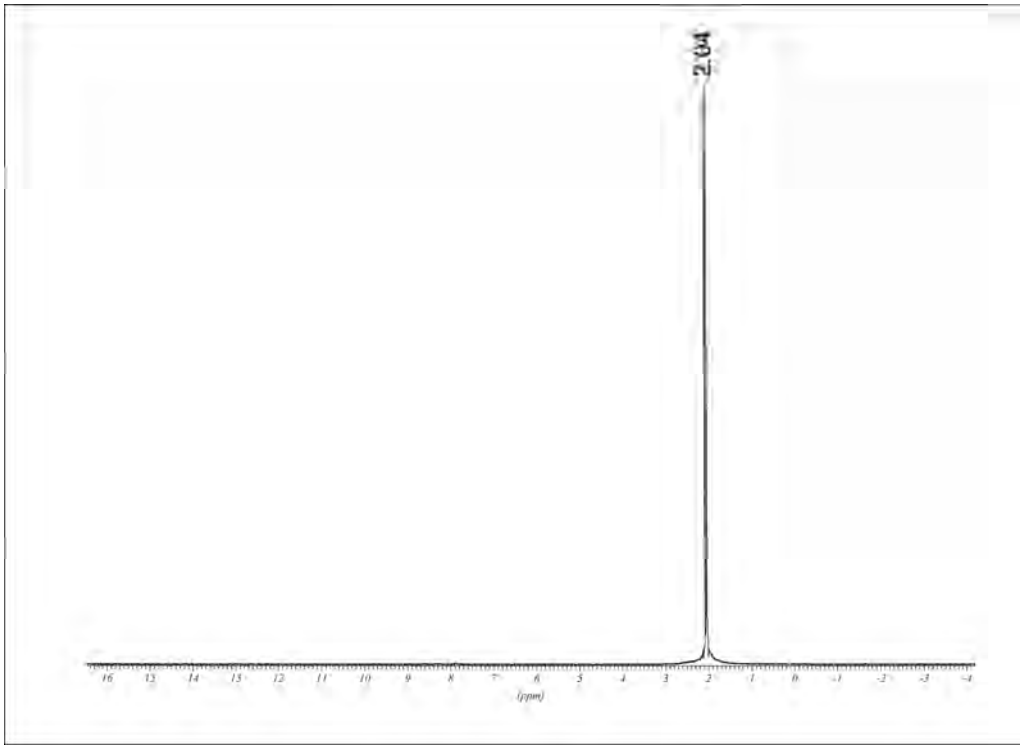

Figure 3.36 ^{1}H NMR spectrum of [$CrCl_3$(bipy)(py)] in acetone-d_6

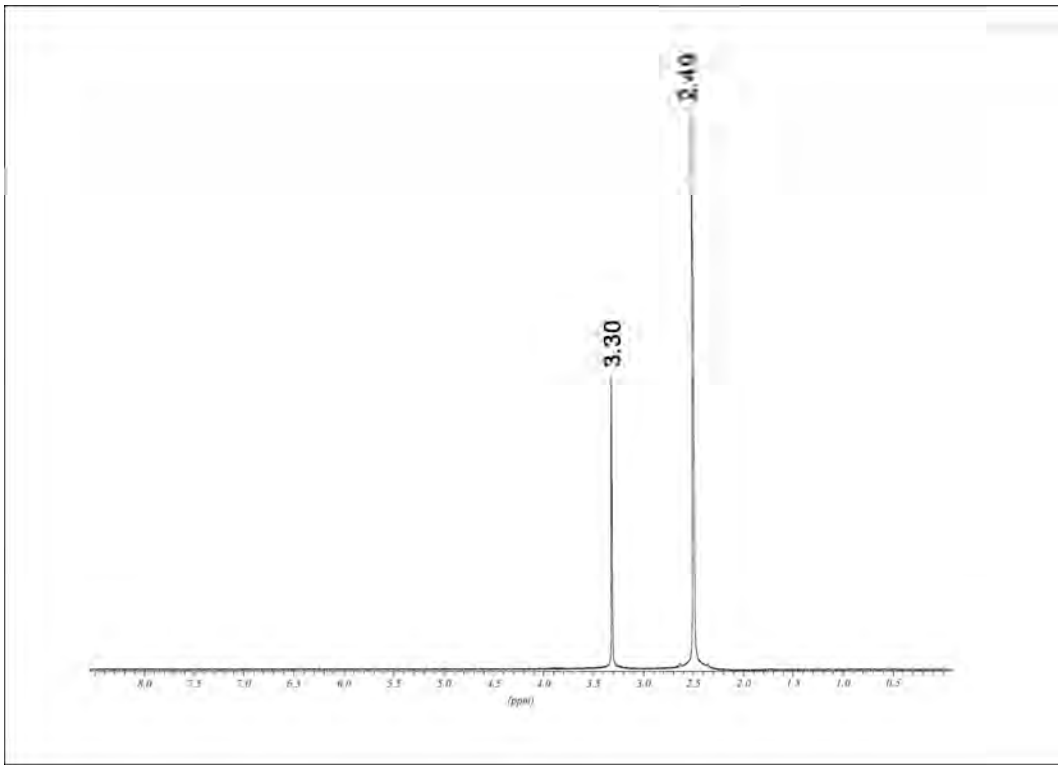

Figure 3.37 ^{1}H NMR spectrum of [$CrCl_3$(bipy)(H_2O)] in DMSO-d_6

3.7 MASS SPECTROMETRY

As was the case for the computational analysis, a representative selection of the compounds were analysed by FAB-MS. These included [$CrCl_3$(bipy)(thf)], [$CrCl_3$(bipy)(H_2O)], [$CrCl_3$(bipy)(CH_3CN)] and [$CrCl_3$(bipy)(pyphenyl)].

In conjunction with the vibrational results the FAB-MS spectrum of the [$CrCl_3$(bipy)(thf)] precipitate suggests the monomeric species. The isotopic distribution patterns for $[M–thfCl]^+$ (m/z = 278) and $[M–thfH2Cl]^+$ (m/z = 243) fragments are observed and correspond with the equivalent theoretically generated patterns. See Figure 3.38.

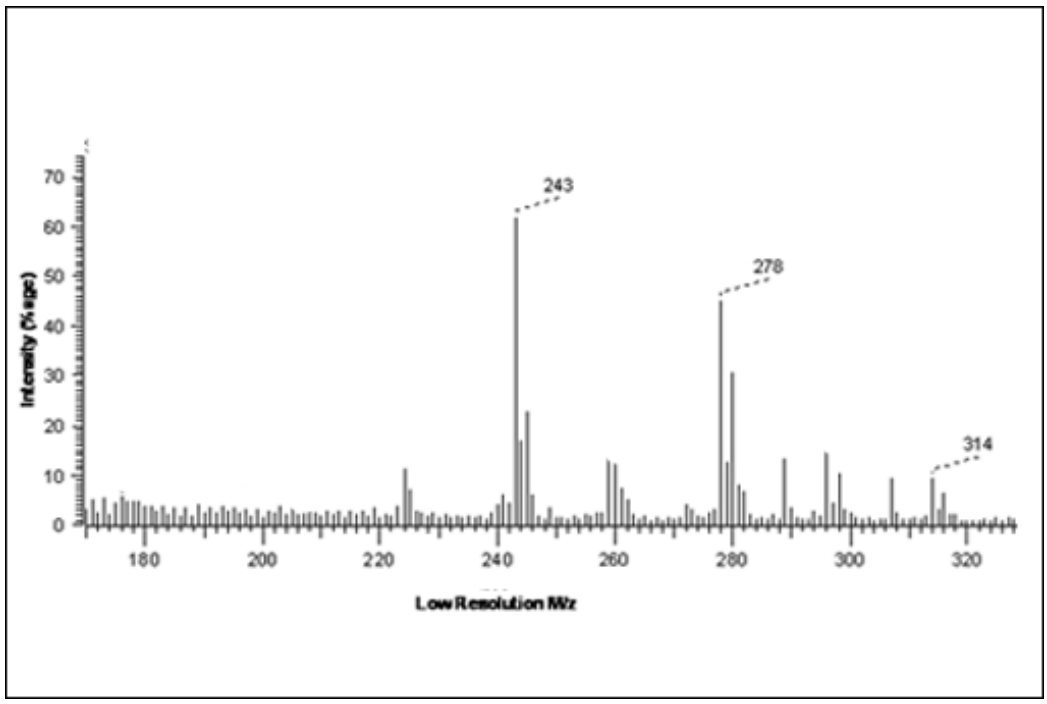

Figure 3.38 FAB-MS spectrum of [$CrCl_3$(bipy)(thf)]

The mass spectrum of the [$CrCl_3$(bipy)(H_2O)] precipitate is shown in Figure 3.39 and corresponds with the structure elucidated from the single crystal determination. Well defined isotopic distribution patterns are observed for the $[M–Cl]^+$ (m/z = 296) and $[M–H_2OCl]^+$ (m/z = 278) fragments and these are in agreement with the theoretical equivalents.

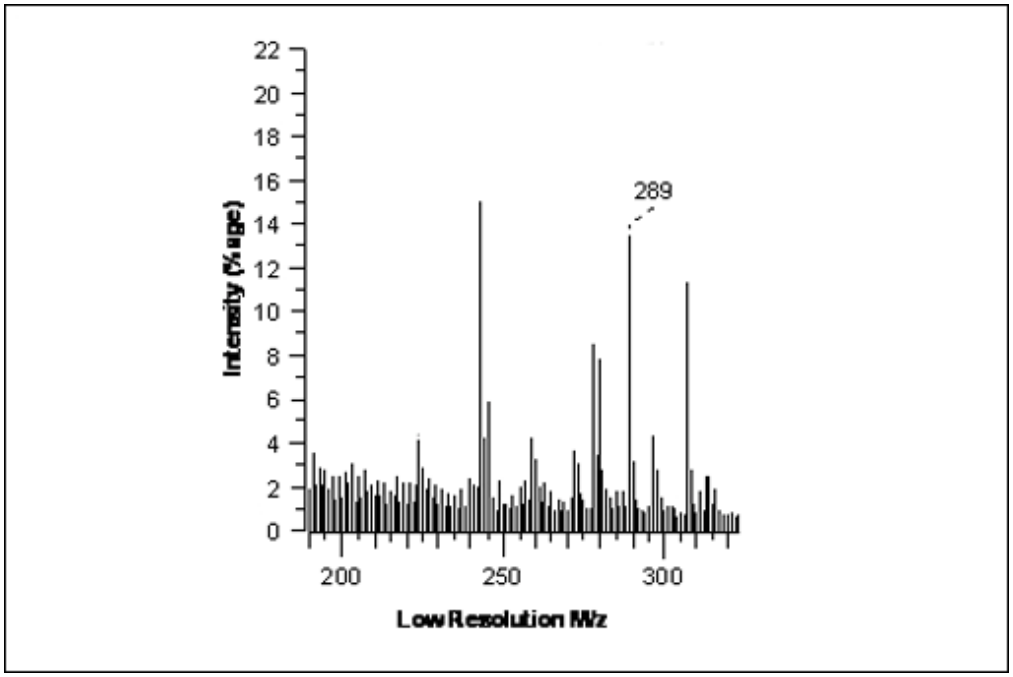

Figure 3.39 FAB-MS spectrum of [$CrCl_3$(bipy)(H_2O)]

The molecular fragments $[M–CH_3CNCl]^+$ (m/z = 278) and $[M–CH_3CN2Cl]^+$ (m/z = 243) are observed for the precipitate of [$CrCl_3$(bipy)(CH_3CN)] (see Figure 2.40) and are confirmed by good isotopic patterns which correlate with those calculated theoretically. Based on the MS results of the other compounds within this class these fragments are associated with the monomeric species.

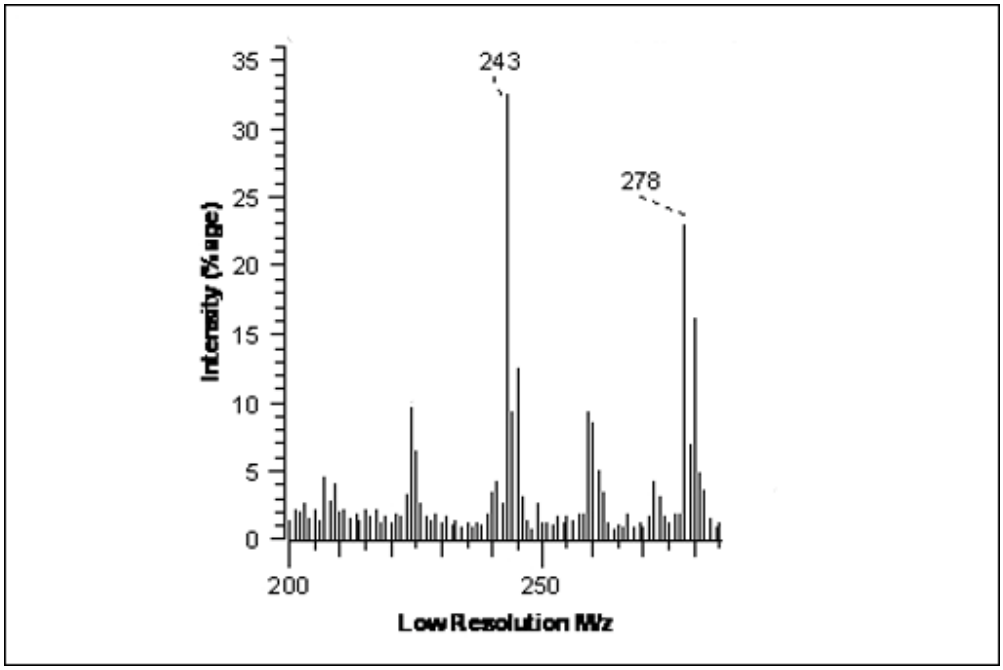

Figure 3.40 FAB-MS spectrum of [$CrCl_3$(bipy)(CH_3CN)]

Confirmation of the monomeric species as defined by the vibrational analysis is seen in the MS spectrum of the [$CrCl_3$(bipy)(pyphenyl)] precipitate in Figure 3.41. Isotopic distribution patterns that correlate to those generated by the isotopic calculator include $[M–Cl]^+$ (m/z = 433), $[M–pyphenylCl]^+$ (m/z = 278) and $[M–pyphenyl2Cl]^+$ (m/z = 243).

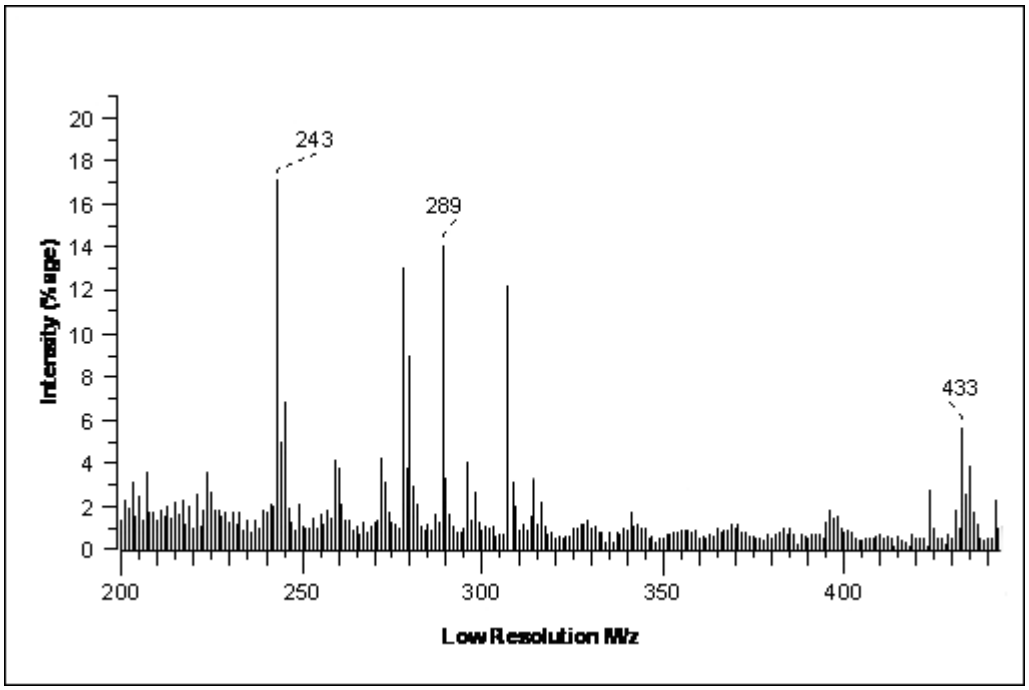

Figure 3.41 FAB-MS spectrum of [$CrCl_3$(bipy)(pyphenyl)]

3.8 X-RAY CRYSTALLOGRAPHY

3.8.1 SOLUBILITY AND CRYSTAL SYNTHESIS

As with the class of compounds discussed in the previous chapter, solubility once again proved problematic and the growing of suitably sized crystals was both a difficult and at times a frustrating practice. Of the wide array of solvents tested to carry out crystallisation, only four successfully dissolved the precipitates to a suitable degree. Perhaps unsurprisingly, these included the highly polar solvents DMSO and DMF with dielectric constants of 47.2 and 38.3 respectively. Although crystals have previously been grown from these solvents, not least the compound [$CrCl_3(py)_2$(DMF)] in the previous chapter, they are not normally regarded as the

solvents of choice for crystallisation as their high vapour pressures inhibit evaporation.

The successful crystallisations were achieved by the slow evaporation of the solvents CH_3CN (dielectric constant of 37.5) and $ClCH_2CN$ (dielectric constant of 30) to yield $[CrCl_3(bipy)(H_2O)]$ and $[HpyNH_2][CrCl_4(bipy)]$ respectively. $ClCH_2CN$ was certainly the better of the two solvents in terms of solubility. The author ascribes this to the increased polarity attributed to the addition of the chlorine atom. Although there was only sparing solubility in CH_3CN, the filtering of a saturated CH_3CN solution proved successful in yielding suitable crystals.

3.8.2 $[CrCl_3(bipy)(H_2O]$

As previously mentioned in regard to the early investigation into the synthesis of $[CrCl_3(thf)_3]$ in Chapter 1, the crystal structure of $[CrCl_3(bipy)(H_2O)]$ resulted from the reaction between bipyridine and water-contaminated $[CrCl_3(thf)_3]$. It is worth mentioning, however, that a precipitate of $[CrCl_3(bipy)(H_2O)]$ was synthesised by the addition of a few drops of water to a $[CrCl_3(bipy)(thf)]$ reaction mixture which used Sigma Aldrich grade $[CrCl_3(thf)_3]$. IR characterisation of the precipitate revealed a spectrum identical to that of the H_2O-coordinated crystal structure.

Although the molecular structure of complex $[CrCl_3(bipy)(H_2O)]$ is similar to that reported for aqua-(4,4'–t–butyl–2,2'–bipyridyl) trichlorochromium(III) tetrahydrofuran solvate by Namba [108], there are significant crystallographic differences between the two structures. Figure 3.42 shows the perspective drawings of the two structures.

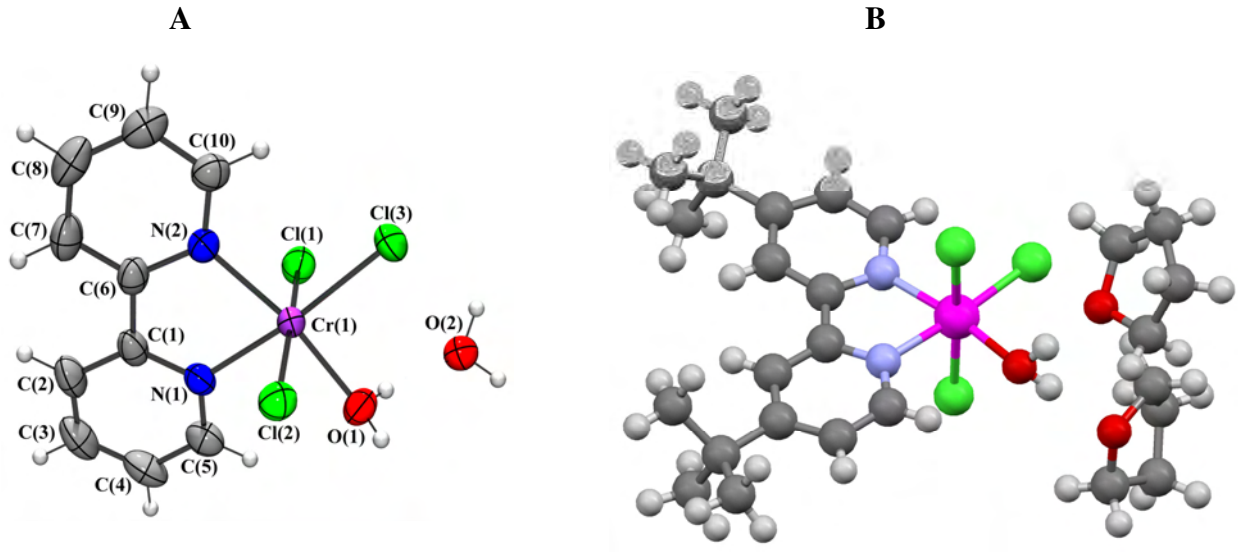

Figure 3.42 **A = Perspective drawing of [$CrCl_3(bipy)(H_2O)$] structure determined in this study, B = Perspective drawing of the structure determined by Namba [108]**

In both structures the chromium atom is coordinated to three chlorine atoms, the two nitrogen atoms of the bipyridine group and the oxygen atom of a water ligand. The water ligand is *trans* to one of the bipyridine nitrogen atoms in both structures. In [$CrCl_3(bipy)(H_2O)$] the coordination is approximately octahedral, with the largest deviation being the N–Cr–N bond angle (78.79(9)°). This is a significantly greater deviation than was observed for the pyridine structures of Chapter 2 and is a direct result of the five–membered chelate ring. Note that all the other *cis* Cr-centred bond angles are in the range 85.16(6) to 95.70(7)° (see Table 3.17). The slight shortening of the Cr–N bond lengths relative to the monodentate analogues was also observed and is also a direct consequence of the bipyridine-induced chelate ring.

To continue the comparison with the 'Namba structure', it was observed that the bipyridine ligands in both complexes are non–planar. The degree of twisting between the two ring systems is, however, greater in the unsubstituted bipyridine structure of this study and is clearly seen in the N(1)–C(5)–C(6)–N(2) torsion angle comparisons of 3.9(5)° ('Namba structure') and 9.0(3)° (this study).

Table 3.17 **Selected bond lengths [Å], bond angles [°] and torsion angles [°] for [$CrCl_3(bipy)(H_2O)$]**

Cr(1)-O(1)	2.003(2)	Cr(1)-Cl(3)	2.3083(8)
Cr(1)-N(1)	2.059(2)	Cr(1)-Cl(2)	2.3114(8)
Cr(1)-N(2)	2.066(2)	Cr(1)-Cl(1)	2.3435(8)
O(1)-Cr(1)-N(1)	92.28(9)	N(2)-Cr(1)-Cl(2)	89.74(6)
N(1)-Cr(1)-N(2)	78.79(9)	Cl(3)-Cr(1)-Cl(2)	93.26(3)
O(1)-Cr(1)-Cl(3)	93.31(7)	O(1)-Cr(1)-Cl(1)	88.28(7)
N(2)-Cr(1)-Cl(3)	95.70(7)	N(1)-Cr(1)-Cl(1)	85.16(6)
O(1)-Cr(1)-Cl(2)	87.50(7)	N(2)-Cr(1)-Cl(1)	93.46(6)
N(1)-Cr(1)-Cl(2)	88.83(6)	Cl(3)-Cr(1)-Cl(1)	93.16(3)
N(1)-C(1)-C(6)-N(2)	9.0(3)	C(2)-C(1)-C(6)-C(7)	10.8(4)

Table 3.18 highlights the differences of structural importance.

Table 3.18 **Crystallographic differences between the two structures**

Crystal data	**[$CrCl_3(bipy)(H_2O)$]**	**Namba structure[109]**
Crystal system	Monoclinic	Orthorhombic
Space group	C 2/c	P $2_12_12_1$
Volume/non-H atoms	19.1 $Å^3$	21.6 $Å^3$
R-factor	3.51%	6.97%

As both structures possess different solvent molecules within their respective unit cells, variations are also observed regarding solvent–complex interactions. In fact, a comparison between the volumes/non-H atoms of the two structures, as documented in Table 3.18, suggests that there is more efficient packing in the structure of this study as a result of stronger intermolecular interactions. The hydrogen bond interactions within the [$CrCl_3(bipy)(H_2O)$] complex will now be discussed in detail.

The oxygen atom of the non–coordinated water molecule lies on a crystallographic twofold rotation axis. Both the coordinated and non–coordinated water molecules,

together with two of the chlorine atoms (Cl(1) and Cl(3)), are involved in an extended network of hydrogen bonds (see Figure 3.43 and Table 3.19). Each non–coordinated water molecule is involved in four hydrogen bonds: two as a donor to two symmetry–related Cl(1) atoms and two as an acceptor from two symmetry–related coordinated water molecules. Each coordinated water molecule is involved in two hydrogen bonds: as a donor to both a non–coordinated water molecule and a symmetry–related Cl(3) atom.

Table 3.19 **Hydrogen bonds for [$CrCl_3(bipy)(H_2O)$] [Å and °]**

D-H...A	d(D-H)	d(H...A)	d(D...A)	<(DHA)
O(1)-H(1B)...O(2)	0.72(4)	1.98(4)	2.690(3)	173(4)
O(1)-H(1A)...Cl(3)#1	0.80(3)	2.40(4)	3.192(2)	176(3)
O(2)-H(2A)...Cl(1)#1	0.84(3)	2.39(3)	3.1671(17)	156(3)

Symmetry transformations used to generate equivalent atoms:
#1 x,-y,z-1/2

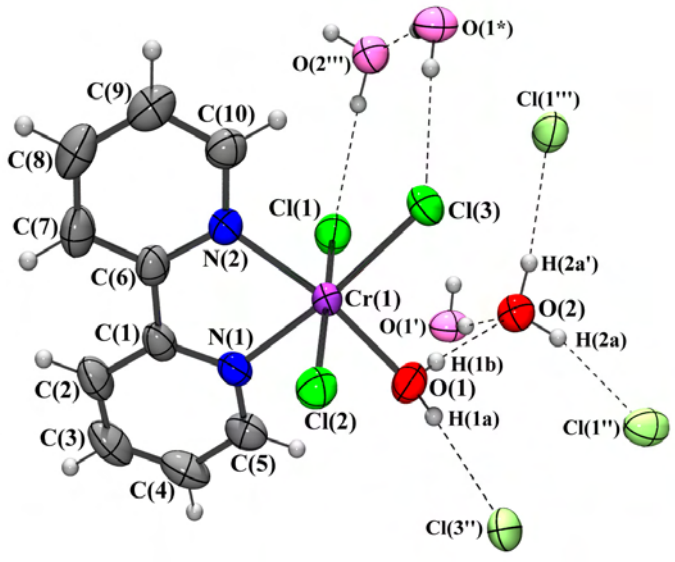

Figure 3.43 **Hydrogen bond interactions**

The final difference between the two structures is observed in their respective packing arrangements, with only [$CrCl_3(bipy)(H_2O)$] possessing short-contact interactions between the aromatic ring layers. They are best described as staggered π–π interactions with a maximum distance of 3.379 Å. See Figure 3.44.

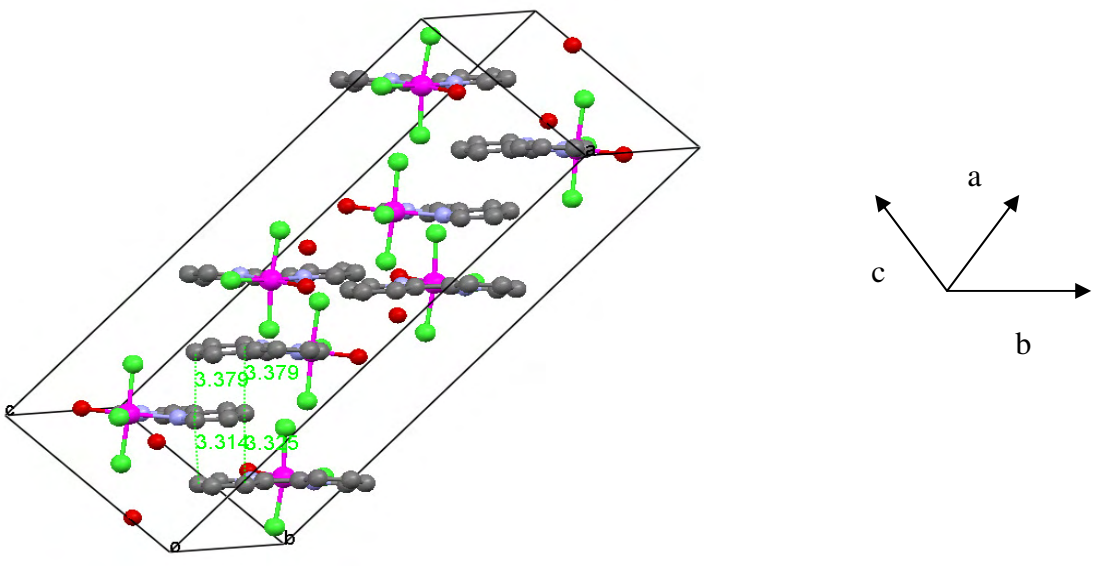

Figure 3.44 Short contacts between aromatic ring layers

In addition, the powder X–ray diffraction pattern of [$CrCl_3(bipy)(H_2O)$] calculated from the crystal structure was compared with the experimentally obtained powder X-ray diffraction pattern; the excellent agreement is shown in Figure 3.45.

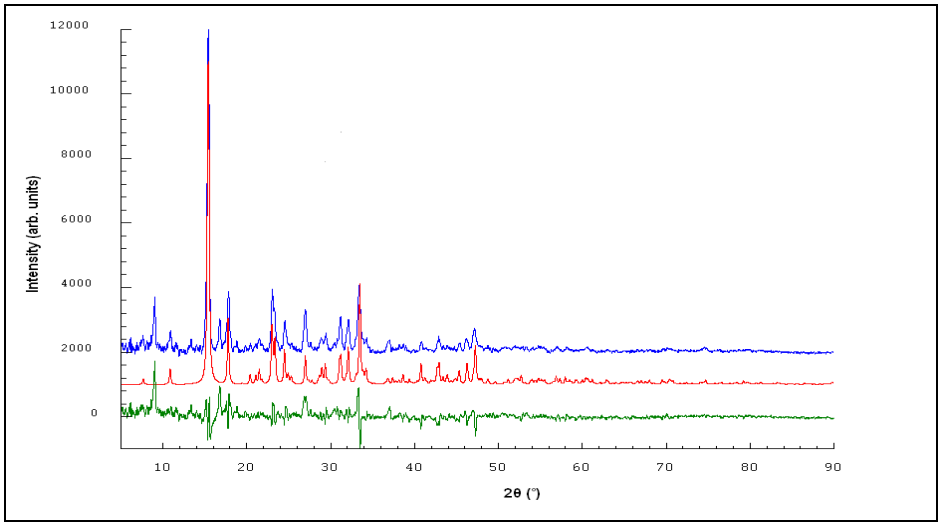

RED: Calculated BLUE: Single crystal sample GREEN: Difference

Figure 3.45 Comparison of the experimental and theoretically obtained X-ray diffraction powder patterns of [$CrCl_3(bipy)(H_2O)$]

Table 3.20 Crystal data and structure refinement for [$CrCl_3$(bipy)(H_2O)].

Empirical formula	$C_{10}\ H_{11}\ Cl_3\ Cr\ N_2\ O_{1.5}$	
Formula weight	341.56	
Temperature	293(2) K	
Wavelength	0.71073 Å	
Crystal system	Monoclinic	
Space group	C 2/c	
Unit cell dimensions	a = 27.034(3) Å	α= 90°
	b = 10.1086(12) Å	β= 97.371(2)°
	c = 9.8700(12) Å	γ = 90°
Volume	2674.9(6) $Å^3$	
Z	8	
Density (calculated)	1.696 Mg/m^3	
Absorption coefficient	1.443 mm^{-1}	
F(000)	1 376	
Crystal size	0.38 x 0.20 x 0.18 mm^3	
Theta range for data collection	2.93 to 26.37°	
Index ranges	-33<=h<=33, -9<=k<=11, -12<=l<=5	
Reflections collected	6 715	
Independent reflections	2 486 [R(int) = 0.0262]	
Completeness to theta = 25.00°	99.2%	
Absorption correction	Semi-empirical from equivalents	
Max. and min. transmission	0.771 and 0.540	
Refinement method	Full-matrix least-squares on F^2	
Data / restraints / parameters	2 486 / 0 / 168	
Goodness-of-fit on F^2	1.091	
Final R indices [I>2σ(I)]	R1 = 0.0351, wR2 = 0.0921	
R indices (all data)	R1 = 0.0437, wR2 = 0.1011	
Extinction coefficient	0	
Largest diff. peak and hole	0.478 and -0.387 e.$Å^{-3}$	

3.8.3 [$HpyNH_2$][$CrCl_4$(bipy)]

The [$HpyNH_2$][$CrCl_4$(bipy)] structure was isolated from the reaction in which bipyridine and $pyNH_2$ were both added to the chromium precursor in thf and stirred overnight. The resulting precipitate was dissolved in $ClCH_2CN$ and after a period of three days, a relatively large number of suitably sized crystals was observed.

[$HpyNH_2$][$CrCl_4$(bipy)] crystallises in an orthorhombic space group, Pnnm. The molecular structure is shown in Figure 3.46 and represents the only known structure of a bipy tetrachloro chromium complex anion. However, the coordination geometry is similar to that of the complex anion in the published structure of benzyl triphenylphosphonium tetrachloro (1,2–phenylenediamine N,N) chromium(III) dichloromethane solvate [109]. A certain degree of comparison can also be made with the previously solved Cr–bipyridine structure, [$CrCl_3$(bipy)(H_2O)].

The chromium atom is coordinated to four chlorine atoms and the two nitrogen atoms of the bipyridine ligand. The coordination is approximately octahedral with the largest deviation being the N(1)–Cr(1)–N(1)#1 bond angle (78.02(14)°) which is, as expected, very similar to other Cr–bipyridine structures. All the other *cis* X–Cr–Y bond angles are in the range 86.63(7) to 94.23(7)° (see Table 3.21). The dihedral angle between the mean planes through each of the two rings comprising the bipyridine ligand is 4.63(10)°. Unlike the novel structure above, the bipyridine ligand is observed as planar, with the N(1)–C(1)–C(10)–N(10) torsion angle constrained by symmetry to be 0°.

The metal–ligand bond lengths can be seen in Table 3.21, with both the Cr–N and Cr-Cl distances being comparable to those of [$CrCl_3$(bipy)(H_2O)].

Table 3.21 Selected bond lengths [Å] and angles [°] for [$HpyNH_2$][$CrCl_4$(bipy)]

Cr(1)-N(1)	2.088(3)	Cr(1)-Cl(3)	2.3172(9)
Cr(1)-N(1)#1	2.088(3)	Cr(1)-Cl(1)	2.3415(13)
Cr(1)-Cl(3)#1	2.3172(9)	Cr(1)-Cl(2)	2.3515(12)
N(1)-Cr(1)-N(1)#1	78.02(14)	Cl(3)#1-Cr(1)-Cl(1)	93.22(4)

N(1)#1-Cr(1)-Cl(3)#1	94.23(7)	Cl(3)-Cr(1)-Cl(1)	93.22(4)
N(1)-Cr(1)-Cl(3)	94.23(7)	N(1)-Cr(1)-Cl(2)	87.46(7)
Cl(3)#1-Cr(1)-Cl(3)	93.52(5)	N(1)#1-Cr(1)-Cl(2)	87.46(7)
N(1)-Cr(1)-Cl(1)	86.63(7)	Cl(3)#1-Cr(1)-Cl(2)	91.99(4)
N(1)#1-Cr(1)-Cl(1)	86.63(7)	Cl(3)-Cr(1)-Cl(2)	91.99(4)
N(1)-C(1)-C(2)-C(3)	0.0(5)	C(3)-C(4)-C(5)-N(1)	0.0(6)

Symmetry transformations used to generate equivalent atoms:
#1 x, y, -z+1 #2 -x+1, -y+1, z

Interestingly, the pyridinium N–H and amine groups, together with the two *trans* Cl ligands of the complex anion, are involved in an extended network of hydrogen bonds (see Figure 3.46 and Table 3.22). The pyridinium N(2)–H(2N) group is hydrogen bonded to two symmetry–related Cl(2) ligands which are, in turn, hydrogen bonded to a second, symmetry–related N(2)–H(2N) group. The pyridinium amine, N(3)–H(3N), is hydrogen bonded to Cl(1). A crystallographic twofold rotation axis generates the second amine hydrogen and the Cl(1) ligand of a second complex anion to which it is hydrogen bonded. The two Cl(1) ligands are, in turn, also hydrogen bonded to a second pyridinium amine group. There are further weak hydrogen bonds (not shown in Figure 3.46) between the amine hydrogens and the chlorine atoms of the DCM solvate molecules.

Table 3.22 Hydrogen bonds for [HpyNH$_2$][CrCl$_4$(bipy)] [Å and º]

D-H...A	d(D-H)	d(H...A)	d(D...A)	<(DHA)
N(2)-H(2N)...Cl(2)#3	0.76(7)	2.67(5)	3.250(4)	134.9(10)
N(3)-H(3N)...Cl(1)	0.96(7)	2.66(8)	3.278(3)	123(6)
N(3)-H(3N)...Cl(4)#2	0.96(7)	2.80(7)	3.605(3)	142(6)

Symmetry transformations used to generate equivalent atoms:
#1 x ,y, -z+1 #2 -x+1, -y+1, z #3 x+1/2, -y+1/2, -z+1/2

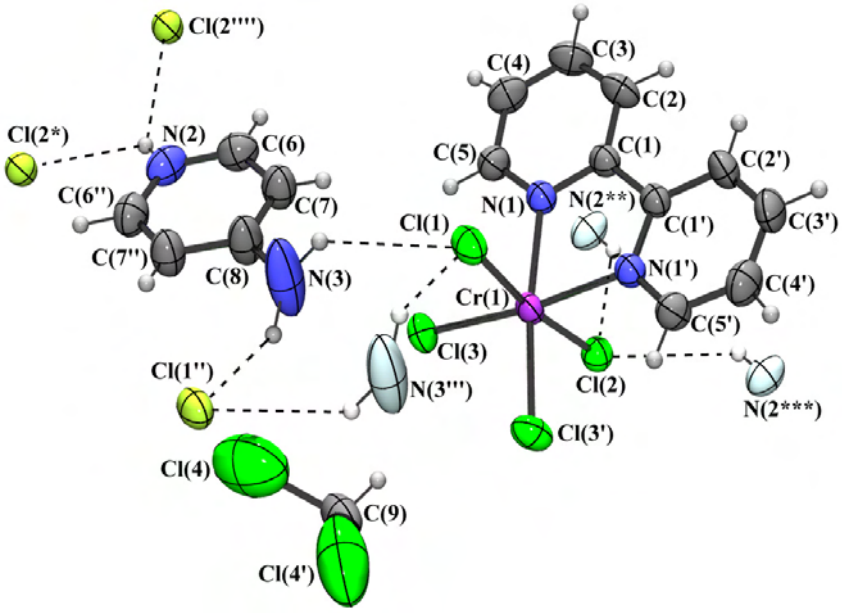

Figure 3.46 Hydrogen bond interactions

Further interactions are observed between the bipyridine and pyridinium ring systems and, as can be seen in Figure 3.47, these are best described as staggered π–π interactions. Figure 3.48 shows a packing and space fill arrangement.

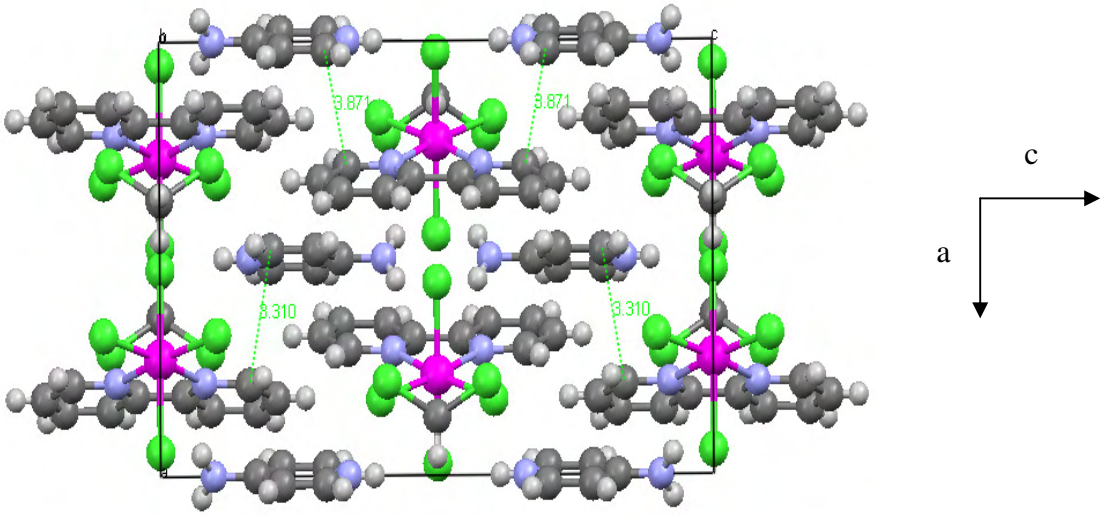

Figure 3.47 Staggered π–π interactions in the packing arrangement of [HpyNH$_2$][CrCl$_4$(bipy)]

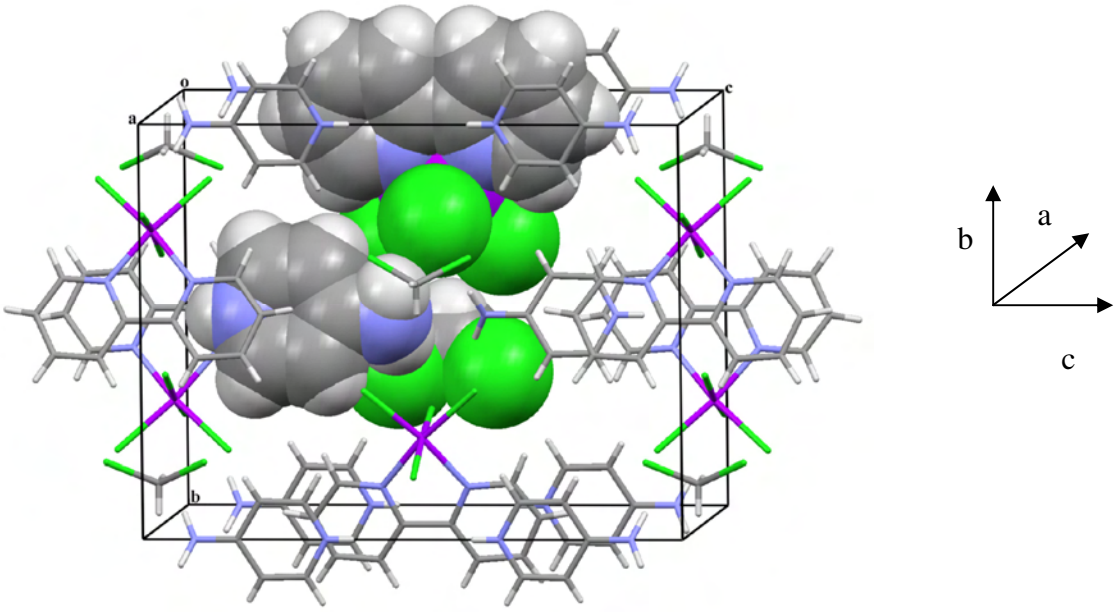

Figure 3.48 **Packing and space fill of $[HpyNH_2][CrCl_4(bipy)]$**

Table 3.23 **Crystal data and structure refinement for $[HpyNH_2][CrCl_4(bipy)]$**

Empirical formula	$C_{16}\ H_{17}\ Cl_6\ Cr\ N_4$	
Formula weight	530.04	
Temperature	293(2) K	
Wavelength	0.71073 Å	
Crystal system	Orthorhombic	
Space group	P n n m	
Unit cell dimensions	a = 10.4815(5) Å	α= 90º.
	b = 12.6236(6) Å	β= 90º.
	c = 16.4879(8) Å	γ = 90º.
Volume	2181.58(18) $Å^3$	
Z	4	
Density (calculated)	1.614 Mg/m^3	
Absorption coefficient	1.269 mm^{-1}	
F(000)	1 068	
Crystal size	0.32 x 0.26 x 0.15 mm^3	
Theta range for data collection	2.47 to 26.52º.	
Index ranges	-13<=h<=4, -14<=k<=15, -19<=l<=20	
Reflections collected	11 301	

Independent reflections	2 235 [R(int) = 0.0350]
Completeness to theta = 25.00º	99.9%
Absorption correction	Semi-empirical from equivalents
Max. and min. transmission	0.827 and 0.635
Refinement method	Full-matrix least-squares on F^2
Data / restraints / parameters	2 235 / 0 / 163
Goodness-of-fit on F^2	1.046
Final R indices [I>2σ(I)]	R1 = 0.0480, wR2 = 0.1327
R indices (all data)	R1 = 0.0543, wR2 = 0.1424
Extinction coefficient	0
Largest diff. peak and hole	0.693 and -1.079 e.Å^{-3}

3.8.4 $[CrCl_2(bipy)_2][Cl]\cdot H_2O$

The above two novel structures were obtained by the standard procedure involving the dissolution of precipitates in suitable solvents. This point is emphasised because a third structure was obtained but via a slightly unusual technique. A large excess of bipyridine dissolved in thf was added to a thf solution of $[CrCl_3(thf)_3]$ at room temperature (ratio of bipyridine to $[CrCl_3(thf)_3]$ was 10:1). The mixture was allowed to stand with no stirring of the solution. After about 60 seconds the solution turned green. After a number of days sizable crystals, light brown in colour, resulted. Their crystallographic analysis revealed the previously determined $[CrCl_2(bipy)_2]^+$ with Cl^- counter-ions. $[CrCl_2(bipy)_2][Cl]\cdot H_2O$ crystallises in an orthorhombic space group, Pbca, with two formula units in the asymmetrical unit. This contrasts with the triclinic unit cell reported for the corresponding dihydrate structure (no details of that structure were reported) [110]. Owing to the relatively low quality of the reflection intensity data and the severe disorder of the chloride anions and water molecules, the structural and geometrical parameters of the complex cations are of somewhat low precision. Regrettably, it was not possible to obtain any better crystals.

As expected, the complex cations have a *cis* arrangement of the chlorine ligands (see Figure 3.49). This arrangement and the bonding geometry of the cations are

comparable to those recently reported for the same complex cation in *cis* [Cr(2,2'–bipy)$_2$Cl$_2$](Cl)$_{0.38}$(PF$_6$)$_{0.62}$ [111].

The largest deviation from the octahedral coordination in [CrCl$_2$(bipy)$_2$][Cl] is the N(8)–Cr(2)–N(7) angle of 78.4(3)°, while all other *cis* X–Cr–Y bond angles are in the range 78.6(2) to 96.9(2)° (see Table 3.23).

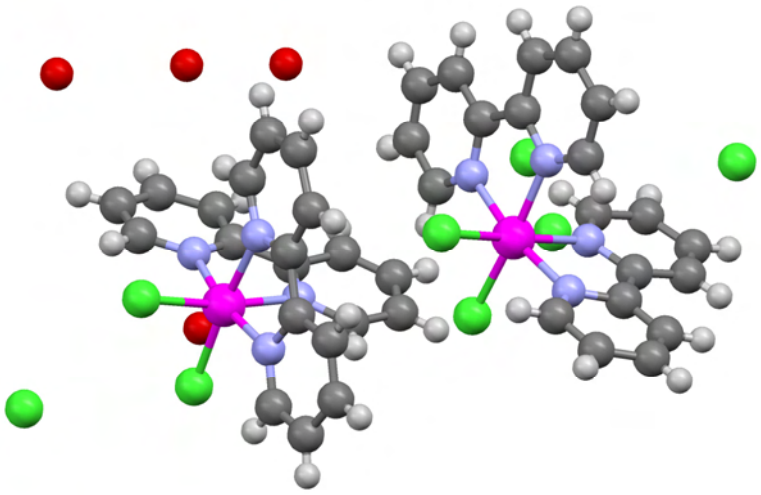

Figure 3.49 **Perspective drawing showing the two formula units of [CrCl$_2$(bipy)$_2$][Cl]·H$_2$O in the asymmetric unit**

The metal–ligand bond lengths are also very similar in the two structures (as would be expected), and only slight differences are observed in their bipyridine ring torsion angles. The greatest difference is observed between the equivalent N(3)–C(11)–C(16)–N(4) of this study and N(2)–C(6)–C(5)–N(1) from the literature, with a difference of 4.27°.

The major differences between the structures are with respect to structural and refinement data. These differences are highlighted in Table 3.24.

Table 3.24 Crystallographic differences between the two structures

Crystal data	$[CrCl_2(bipy)_2][Cl]\cdot H_2O$	$[CrCl_2(bipy)_2][PF_6]$ [111]
Crystal system	Orthorhombic	Monoclinic
Space group	Pbca	C2/c
Volume/non-H atoms	21.2 $Å^3$	17.2 $Å^3$
R-factor	8.75%	5.15%

As a consequence of the differing structural data and indeed the volumes/non-H atoms, it is not surprising that the packing arrangements are also different. Figures 3.50 and 3.51 illustrate the packing order and space fill arrangements of $[CrCl_2(bipy)_2][Cl]$.

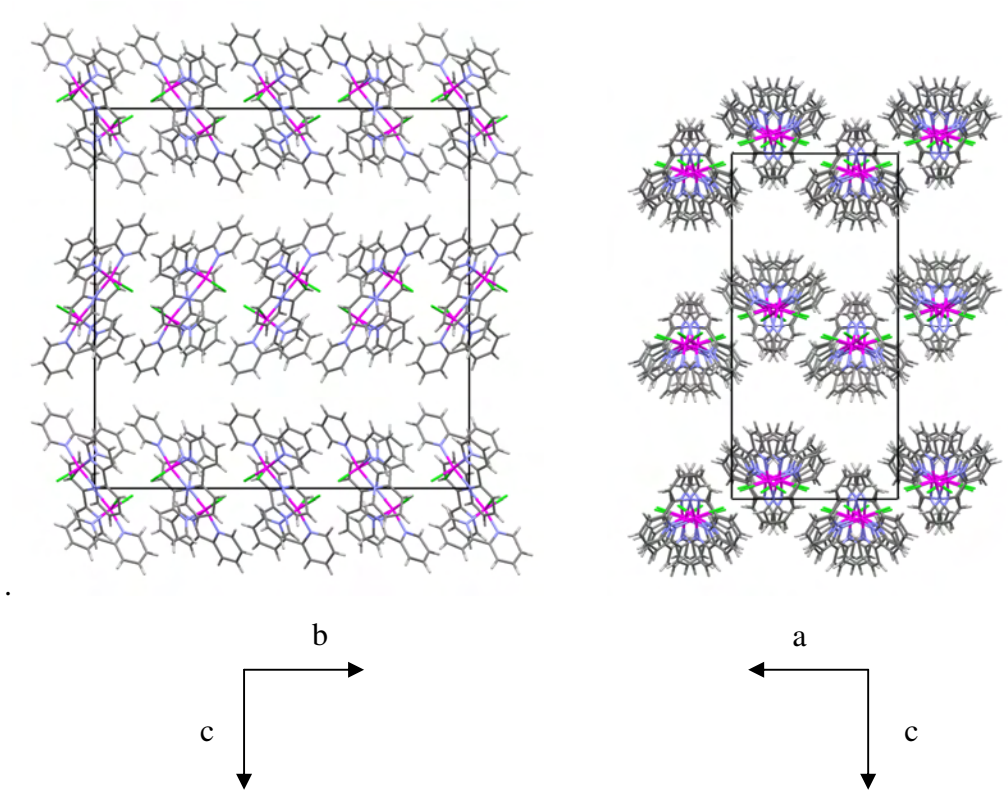

Figure 3.50 Packing arrangements for $[CrCl_2(bipy)_2][Cl]\cdot H_2O$

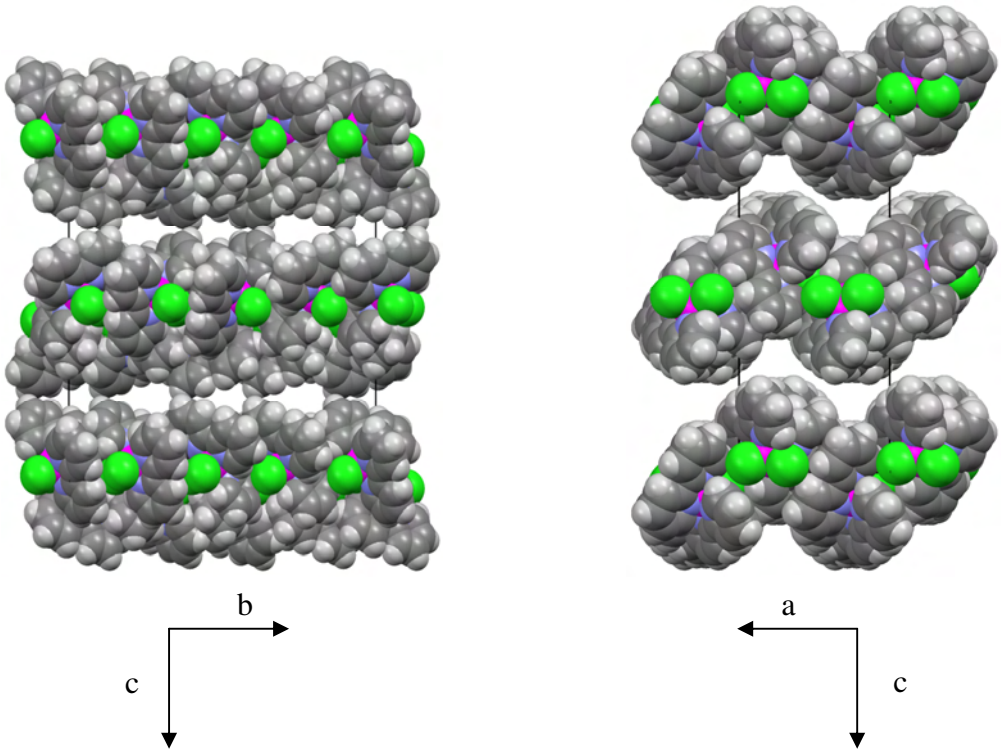

Figure 3.51 **Packing and space fill arrangements for $[CrCl_2(bipy)_2][Cl]\cdot H_2O$**

Table 3.25 **Bond lengths [Å] and angles [°] for $[CrCl_2(bipy)_2][Cl]\cdot H_2O$**

Cr(1)-N(1)	2.063(6)	Cr(1)-N(3)	2.068(5)
Cr(1)-N(2)	2.065(6)	Cr(1)-Cl(1)	2.285(2)
Cr(1)-N(4)	2.065(6)	Cr(1)-Cl(2)	2.2906(18)
N(1)-Cr(1)-N(2)	79.1(3)	N(8)-Cr(2)-N(7)	78.4(3)
N(1)-Cr(1)-N(4)	94.0(2)	N(6)-Cr(2)-N(7)	92.7(2)
N(1)-Cr(1)-N(3)	87.5(2)	N(8)-Cr(2)-N(5)	94.5(2)
N(2)-Cr(1)-N(3)	93.7(2)	N(6)-Cr(2)-N(5)	79.2(2)
N(4)-Cr(1)-N(3)	78.6(2)	N(7)-Cr(2)-N(5)	86.8(2)
N(2)-Cr(1)-Cl(1)	94.2(2)	N(8)-Cr(2)-Cl(3)	89.75(18)
N(4)-Cr(1)-Cl(1)	92.42(16)	N(6)-Cr(2)-Cl(3)	96.10(18)
N(3)-Cr(1)-Cl(1)	91.63(16)	N(7)-Cr(2)-Cl(3)	90.97(17)
N(1)-Cr(1)-Cl(2)	86.92(15)	N(8)-Cr(2)-Cl(4)	96.9(2)
N(2)-Cr(1)-Cl(2)	92.36(16)	N(6)-Cr(2)-Cl(4)	91.30(17)
N(4)-Cr(1)-Cl(2)	94.57(16)	N(5)-Cr(2)-Cl(4)	87.05(16)
Cl(1)-Cr(1)-Cl(2)	94.79(8)	Cl(3)-Cr(2)-Cl(4)	95.61(9)

N(1)-C(1)-C(6)-N(2)	3.9(10)	N(5)-C(21)-C(26)-N(6)	-2.8(8)
C(2)-C(1)-C(6)-C(7)	5.9(14)	C(22)-C(21)-C(26)-C(27)	-5.1(11)
N(3)-C(11)-C(16)-N(4)	0.4(8)	N(7)-C(31)-C(36)-N(8)	5.4(10)
C(12)-C(11)-C(16)-C(17)	-1.3(11)	C(32)-C(31)-C(36)-C(37)	6.3(13)

Table 3.26 Crystal data and structure refinement for $[CrCl_2(bipy)_2][Cl]\cdot H_2O$

Empirical formula	$C_{40}\ H_{32}\ Cl_6\ Cr_2\ N_8\ O_5$	
Formula weight	1 021.44	
Temperature	297(2) K	
Wavelength	0.71073 Å	
Crystal system	Orthorhombic	
Space group	P b c a	
Unit cell dimensions	a = 12.0476(8) Å	α = 90°.
	b = 29.148(2) Å	β = 90°.
	c = 29.449(2) Å	γ = 90°.
Volume	10 341.4(13) $Å^3$	
Z	8	
Density (calculated)	1.312 Mg/m^3	
Absorption coefficient	0.776 mm^{-1}	
F(000)	4 144	
Crystal size	0.46 x 0.20 x 0.02 mm^3	
Theta range for data collection	2.50 to 26.56°.	
Index ranges	-5<=h<=15, -35<=k<=36, -33<=l<=36	
Reflections collected	53 636	
Independent reflections	10 104 [R(int) = 0.0651]	
Completeness to theta = 25.00°	99.8%	
Absorption correction	Semi-empirical from equivalents	
Max. and min. transmission	0.985 and 0.712	
Refinement method	Full-matrix least-squares on F^2	
Data / restraints / parameters	10 104 / 0 / 568	
Goodness-of-fit on F^2	1.020	

Final R indices [I>2sigma(I)]	R1 = 0.0875, wR2 = 0.2656
R indices (all data)	R1 = 0.1712, wR2 = 0.3370

3.9 SYNTHETIC ROUTE CONCLUSIONS

When one combines all the evidence of this chapter, a mechanism similar to that of Chapter 2 is portrayed, with some interesting differences.

Direct ligand substitution is certainly a viable pathway to the formation of the neutral monomeric compounds. Unlike the immediate addition of the monodentate pyridine to all three available precursor sites, the addition of bipyridine allowed the isolation of an intermediate compound [$CrCl_3$(bipy)(thf)]. It would then be logical to assume that the secondary ligands simply displace and occupy the remaining site.

This same monomeric species could also have formed by the symmetrical cleavage of a dimeric intermediate, the existence of which is indirectly proven by the crystal structure of [$HpyNH_2$][$CrCl_4$(bipy)]; this had to have resulted from the asymmetrical cleavage of the same dimer. The detailed spectroscopic analysis suggests strongly that complexes of this study are monomeric and thus the addition of the secondary amine appears to break the bridging chloro bond in a symmetrical fashion to afford these compounds.

One cannot, however, ignore the isolation of the ionic complexes of which the structures [$HpyNH_2$][$CrCl_4$(bipy)] and [$CrCl_2(bipy)_2$][Cl]·H_2O were determined. Although not of the same compound, they importantly represent both the cationic and anionic Cr fragments that result from asymmetrical dimeric cleavage. It would appear that the cationic, coordinatively saturated fragment is stabilised by the coordination of a second bidentate bipyridine ligand.

As in Chapter 2, the reason why dimers such as these cleave symmetrically or asymmetrically is still unclear.

Figure 3.52 presents a summary of the routes to complex formation.

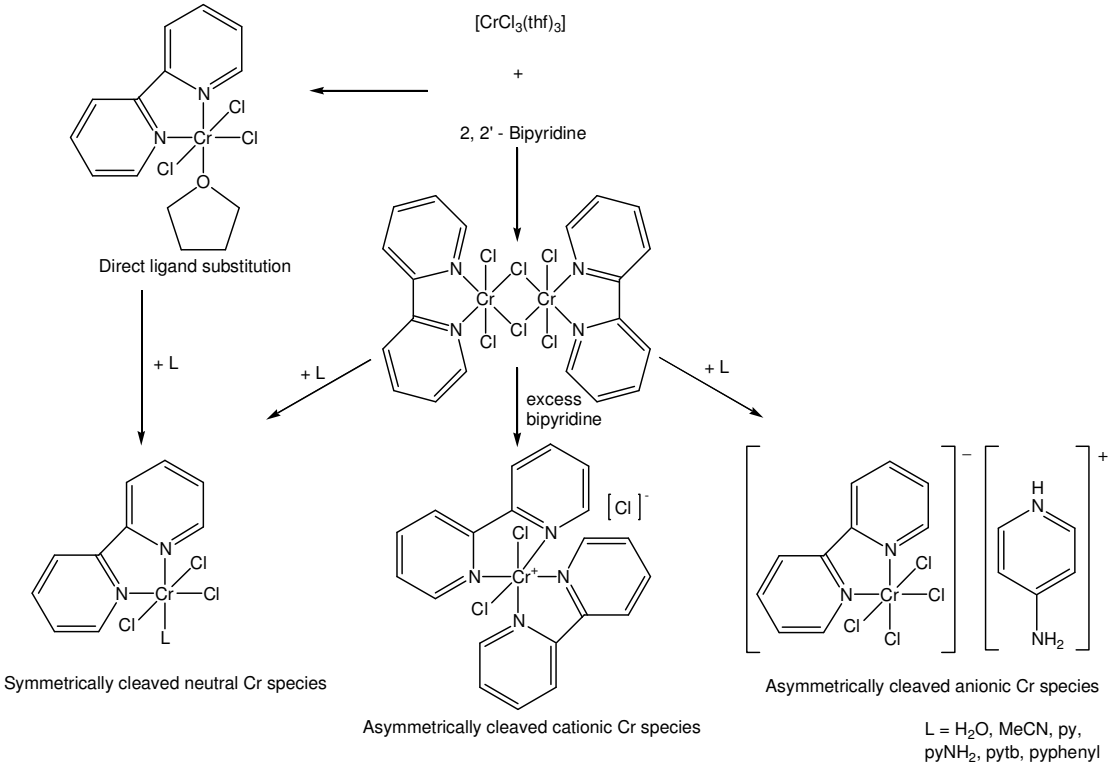

Figure 3.52 Proposed routes to complex formation

3.10 EXPERIMENTAL

3.10.1 SYNTHESIS OF [$CrCl_3$(bipy)(thf)] (9)

A Schlenk tube was charged with [$CrCl_3(thf)_3$] (0.31 g, 0.827 mmol) and thf (30 cm^3). Bipyridine (0.13 g, 0.827 mmol) was then added and the reaction mixture allowed to stir at room temperature. After *ca.* 2 hours the reaction colour was observed as a dark green solution with a light green precipitate starting to form. The reaction was left to stir overnight to ensure completion. The green supernatant solvent was removed via syringe after the crude product had been allowed to settle. The remaining precipitate was subsequently washed with Et_2O (3 x 20 cm^3), the supernatant removed and the final product dried under reduced pressure for 3 hours to afford an olive green solid **(9)** in good yield (0.27 g, 84%).

Repetition of this reaction using water-contaminated [$CrCl_3(thf)_3$] (resulting from the incomplete substitution of water by thf during synthesis from chromium hexahydrate), followed by dissolution in CH_3CN, yielded single crystals of **(16)**.

3.10.2 SYNTHESIS OF [$CrCl_3$(bipy)(CH_3CN)] (10)

A Schlenk tube was charged with [$CrCl_3$(bipy)(thf)] (0.23 g, 0.595 mmol) and CH_3CN (25 cm^3) (where CH_3CN acts as both solvent and N–donor ligand) and stirred overnight at room temperature. The supernatant was removed via syringe, the remaining residue washed with Et_2O (3 x 20 cm^3) and the product dried under reduced pressure for 3 hours. An olive green compound **(10)** was isolated as product (0.15 g, 71%).

3.10.3 SYNTHESIS OF [$CrCl_3$(bipy)(py)] (11)

A Schlenk tube was charged with [$CrCl_3$(bipy)(thf)] (0.21 g, 0.543 mmol) and pyridine (25 cm^3) and stirred at room temperature overnight. Again, the pyridine behaved as solvent and reagent. The supernatant was removed via syringe, and the residue washed with Et_2O (3 x 20 cm^3) and dried under reduced pressure for 3 hours to afford an olive green solid **(11)** as product (0.16 g, 76%).

3.10.4 SYNTHESIS OF [$CrCl_3$(bipy)($pyNH_2$)] (12)

A Schlenk tube was charged with [$CrCl_3(thf)_3$] (0.20 g, 0.534 mmol) and thf (30 cm^3). Bipyridine (0.08 g, 0.534 mmol) was then added and the reaction mixture was carefully monitored. After *ca.* 55 minutes, 4-amino pyridine (0.05 g, 0.534 mmol) was added. The reaction was allowed to stir overnight. The supernatant solvent was removed, the residue washed with Et_2O (3 x 20 cm^3) and the product dried under reduced pressure for 3 hours to afford an olive green solid **(12)** as product (0.15 g, 68%).

Crystals of [$HpyNH_2$][$CrCl_4$(bipy)]CH_2Cl_2 **(15)** were afforded by slow evaporation of [$CrCl_3$(bipy)($pyNH_2$)] in $ClCH_2CN$.

3.10.5 SYNTHESIS OF [$CrCl_3$(bipy)(pytb)] (13)

A Schlenk tube was charged with [$CrCl_3$(bipy)(thf)] (0.26 g, 0.672 mmol) and 4-tert butyl pyridine (20 cm^3) and stirred at room temperature overnight, with the 4-tert butyl pyridine acting as both solvent and reagent. The supernatant was removed, and the remaining residue washed with Et_2O (3 x 20 cm^3) and dried under reduced pressure for 3 hours. An olive green product **(13)** was isolated (0.19 g, 63%).

3.10.6 SYNTHESIS OF [$CrCl_3$(bipy)(pyphenyl)] (14)

A Schlenk tube was charged with [$CrCl_3$ $(thf)_3$] (0.20 g, 0.534 mmol) and thf (30 cm^3). Bipyridine (0.08 g, 0.534 mmol) was then added and the reaction mixture carefully monitored. After *ca.* 1 hour 4-phenyl pyridine (0.08 g, 0.534 mmol) was added and the reaction mixture stirred overnight at room temperature. The supernatant solvent was removed, the residue washed with Et_2O (3 x 20 cm^3) and the product dried under reduced pressure for 3 hours. An olive green product **(14)** was isolated (0.16 g, 64%).

3.10.7 SYNTHESIS OF [$CrCl_3$(bipy)(H_2O)] (16)

A Schlenk tube was charged with [$CrCl_3$(bipy)(thf)] (0.26 g, 0.672 mmol) and thf (30 cm^3). To the reaction 1 ml of distilled water was added. The reaction mixture was left to stir at room temperature overnight. The supernatant was removed via syringe and the product washed with Et_2O (3 x 20 cm^3) and then dried under reduced pressure for 3 hours. An olive green compound **(16)** was isolated as product in good yield (0.21 g, 95%).

3.10.8 SYNTHESIS OF [$CrCl_2(bipy)_2$][Cl]·H_2O (17)

A glass polytop was charged with [$CrCl_3(thf)_3$] (0.05 g, 0.133 mmol) and thf (5 cm^3). To the dissolved solution was added bipyridine (0.2 g, 1.33 mmol) which had been dissolved separately in thf (10 cm^3). The reaction was left to stand without stirring at room temperature. After a period of time large yellow-brown crystals of **(17)** formed.